Current Awareness Bulletin

of

SCHOLARLY ARTICLES PUBLISHED

BY

Faculty, Students and Alumni

~ February 2012 ~

DELHI TECHNOLOGICAL UNIVERSITY CENTRAL LIBRARY
(formerly Delhi College of Engineering, Bawana Road, DELHI)

PREFACE

This is the first Current Awareness Bulletin Service started by Delhi Technological University Library. The aim of the bulletin is to compile, preserve and disseminate information published by the Faculty, Students and Alumni for mutual benefits. The bulletin also aims to propagate the intellectual contribution of DTU as a whole to the academia. It contains information resources available in the internet in the form of articles, reports, presentation published in international journals, websites, etc. by the faculty and students of Delhi Technological University in the field of science and technology. The publication of Faculty and Students which are not covered in this bulletin may be because of the reason that either the full text was not accessible or could not be searched by the search engine used by the library for this purpose. To make the bulletin more comprehensive, the learned faculty and Students may provide their uncovered publication to the library either through email or in CD, etc.

This issue contains the information published during February 2012. The arrangement of the contents is alphabetical wise starting from A-Z. The Full text of the article which is either subscribed by the University or available in the web has been provided in this Bulletin.

CONTENTS

*Faculty
@Students

Edge Detection Using Adaptive Thresholding and Ant Colony Optimization

Om Prakash Verma
Department of Information Technology
Delhi Technological University (Formerly Delhi College of Engineering), Delhi, India.
opverma.dce@gmail.com

Prerna Singhal, Sakshi Garg and Deepti Singh Chauhan
Department of Computer Engineering
Delhi Technological University (Formerly Delhi College of Engineering), Delhi, India.
prerna.singhal90@gmail.com, sakshi.dce08@gmail.com
deepti.s.chauhan@gmail.com

***Abstract*- In this paper, we present an approach for edge detection using adaptive thresholding and Ant Colony Optimization (ACO) algorithm to obtain a well-connected image edge map. Initially, the edge map of the image is obtained using adaptive thresholding. The end points obtained using adaptive threshoding are calculated and the ants are placed at these points. The movement of the ants is guided by the local variation in the pixel intensity values. The probability factor of only undetected neighboring pixels is taken into consideration while moving an ant to the next probable edge pixel. The two stopping rules are implemented to prevent the movement of ants through the pixel already detected using the adoptive thresholding. The results are qualitative analyze using Shanon's Entropy function.**

Keywords-Ant colony optimization, Adaptive thresholding, pheromone, Entropy, End points,

I. INTRODUCTION

An edge can be defined as sudden change of intensity in an image. In binary images, edge corresponds to sudden change in intensity level to 1 from 0 and vice versa. The most of the edge detectors are devised based on this criterion only. In the past years, many algorithms and approaches have been put forward to extract the edges of an image. For example, the Sobel operator is based on convolving the image with a small, separable, and integer valued filter in horizontal and vertical direction. The Prewitt [1] operator calculates the maximum response of a set of convolution kernels to find the local edge orientation for each pixel. The Canny detector [2] uses a multi-stage algorithm to detect a wide range of edges in images and defines edges as zero-crossing of second derivatives in the direction of greatest first derivative. Marr *et al* [3] proposed an algorithm that finds edges at the zero-crossings of the image Laplacian. Non-linear filtering techniques for edge detection also saw much advancement through the SUSAN [4]. However, these methods often result in some drawback like the broken edges which leads to loss of information. Many methods have been proposed in the past to link the broken edges too in order to improve the edge detection. In some approaches, Hough transformation [1, 5] is performed and specific shape is extracted to link the broken edges. However, the edges do not always have fixed shapes. Some other methods use hybrid techniques [6-7] to connect broken edges.

Ant colony optimization (ACO) is heuristic method that imitates the behavior of real ants to solve the discrete optimization problem [8]. Ant colony optimization takes inspiration from the foraging behavior of some ant species [9]. A foraging ant deposits a chemical (pheromone) which increases the probability of following the same path by other ants.

The first ACO algorithm, called the *ant system*, was proposed by Dorigo *et al.* [10]. Since then, a number of ACO algorithms have been developed, such as ant colony system [11], Max-Min ant system [12], ant colony algorithm for solving continuous optimization problem [13], an improved ACO for solving the complex combinatorial optimization problem [14-15], a novel fuzzy ant system for edge detection [16], edge improvement by ant colony optimization [17], ant colony optimization and statistical estimation approach to image edge detection [18], adaptive artificial ant colonies for edge detection in digital images [19], are reported in the literature. Recently, O.P. Verma *et al.*[20] have developed an algorithm for edge detection using BF in which direction of movement of bacteria is found using a directional probability matrix derived from ACO.

In the proposed study ant colony optimization is used to link the discontinuities in the edges while the edges are detected by adaptive thresholding [21]. The edge point information supplied by the adaptive thresholding is more than that supplied by the Sobel operator. Therefore the proposed study of applying ACO to the edges extracted from adaptive thresholding gives better results. The ACO methods are an iterative, probabilistic meta-heuristic for finding solutions to combinatorial optimization problems. They are based on the foraging mechanism employed by real ants attempting to find a short path from their nest to a food source.

The rest of the study is organized as follows: Section 2 gives a brief introduction of the ant colony optimization. The proposed technique is presented in Section 3. Section 4 presents experimental results and conclusions are drawn in Section 5.

978-1-4673-0126-8/11/$26.00 ©2011 IEEE

II. ANT COLONY OPTIMIZATION

Ant colony optimization (ACO) is a nature-inspired optimization algorithm that is motivated by the natural foraging behavior of ant species. Ants deposit the pheromone on the ground to mark paths between a food source and their colony. Pheromone is followed by other members of the colony. Over a time, pheromone trails evaporate. The amount of pheromone evaporation depends on the time taken by the ants to travel down the path and back again. The shorter paths get marched over faster. Pheromone densities remain high on shorter paths because pheromone is laid down faster. This positive feedback mechanism eventually leads the ants to follow the shorter paths. It is this natural phenomenon that inspired the development of the ACO metaheuristic.

In the ACO method, artificial ants use virtual pheromone to update their path through the image edges. ACO iteratively find the optimal solution of the target pixels through the movements of a number of ants over the image, by depositing and evaporating the pheromone trail. The probability for the ant's movement from one pixel to another is decided by probability transition matrix.

Establishment of probabilistic transition matrix and pheromone update is the two key issues in the ant colony optimization technique. During the n^{th} construction step, the k^{th} ant moves according to the probabilistic transition matrix defined as [22]:

$$Pij(n) = \frac{(\tau_{ij}^{(n)})^{\alpha}(\eta_{ij})^{\beta}}{\sum_{j\in\Omega_i}(\tau_{ij}^{(n)})^{\alpha}(\eta_{ij})^{\beta}} \qquad (1)$$

where $\tau_{i,j}^{(n)}$ is the pheromone information value of the arc linking the node i to the node j, $\eta_{i,j}$ represents the heuristic information for pixel (x,y) for going from node i to node j which is calculated using Eq. (2) ,and the constants α and β influence the pheromone information and heuristic information, respectively. All the possible neighboring pixels surrounding the central pixel at (x,y) are shown in Fig.1, where I (x,y) represents the intensity value at x,y.

I(x-1,y+1)	I(x,y+1)	I(x+1,y+1)
I(x-1,y)	I(x,y)	I(x+1,y)
I(x-1,y-1)	I(x, y-1)	I(x+1,y-1)

Fig. 1 Pixel (x, y) with its neighborhood pixel

The $\eta_{i,j}$ is calculated as [15]

$$\eta_{ij} = \frac{\max_{ij}\begin{pmatrix} |I(x-1,y-1)-I(x+1,y+1)|, \\ |I(x-1,y+1)-I(x+1,y-1)|, \\ |I(x,y-1)-I(x,y+1)|, \\ |I(x-1,y)-I(x+1,y)| \end{pmatrix}}{\eta_{\max}} \qquad (2)$$

Where η_{ij} is the heuristic information of pixel (x,y) and η_{max} is maximum heuristic value.

Pheromone intensity attracts the ant to follow the paths traversed by other ants. Hence, pheromone is updated twice, once after the movement of each ant and secondly after movement of all the ants. Each time an ant visits a pixel, it immediately performs a local update on the associated pheromone. The $\tau_{i,j}^{(n)}$, is updated by[22]:

$$\tau_{ij}^{(n)} = (1-\Psi).\tau_{ij}^{(n-1)} + \Psi.\tau_{ij}^{(0)} \qquad (3)$$

where ψ ϵ (0,1] is the pheromone decay coefficient which diversifies the search by decreasing the desirability of edges that have already been traversed.

After the movement of all the ants during the construction step pheromone is updated globally using [16]:

$$\tau^{(n)} = \begin{Bmatrix} (1-\rho).\tau^{(n-1)} + \rho.\Delta\tau^{(k)} if\,(i,j) besttour, \\ \tau^{(n-1)}, otherwise \end{Bmatrix} \qquad (4)$$

where ρ ϵ (0,1] is the evaporation constant. ρ decreases the pheromone value related to the bad solution and thus prevents premature convergence to sub-optimal solutions. $\Delta\tau^{(k)}$is the amount of pheromone deposited by the ant which is given as follows[23]:

$$\Delta\tau^{(k)} = \frac{C}{L^k} \qquad (5)$$

whereL^k is the path length travelled by the k^{th}ant and C is a constant.

III. PROPOSED APPROACH

In the proposed approach, initially edges are extracted using adaptive thresholding. The connectivity of the edges so obtained is then increased using modified ACO.

3.1 Edge Detection using Adaptive Thresholding

Like global thresholding, the adaptive thresholding is used to separate desirable foreground image objects from the background based on the difference in pixel intensities of each region. Global thresholding uses a fixed threshold for all pixels in the image and therefore cannot deal with images containing a varying intensity gradient. Local adaptive thresholding, on the other hand, selects an individual threshold for each pixel based on the range of intensity values in its local neighbourhood.

Adaptive thresholding typically takes a gray scale or color image as input and, in the simplest implementation, outputs a binary image representing the edge information. For each pixel in the image, a threshold has to be calculated. If the pixel value is below the threshold it is set to the background value, otherwise it assumes the foreground value. The flowchart for edge detection using adaptive thresholding is shown in Fig.2.

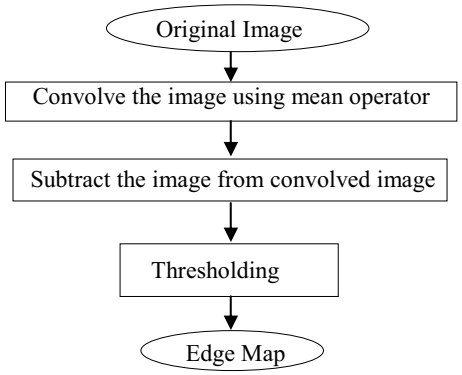

Fig.2 Flowchart for edge detection using adaptive thresholding

The edges obtained using above method contains some thick edges also therefore a thinning algorithm is implemented for the pre-processing for an efficient end point analysis [24]. The

processed image is then analysed to obtain the end point information of the broken edges. The edges extracted from the above steps provide larger end point information as compared with that provided by Sobel operator.

3.2 Edge Improvement

Several discontinuities appear in the image after the application of adoptive thresholding. All the possible neighboring pixels surrounding the central pixel at (x,y) are shown in Fig 2. A central pixel position (x, y) is considered as the endpoint if only one (out of eight) of the neighboring pixels is white and the central pixel itself is also white. This is shown in Fig. 3, where the position (x, y) is the end point. A number of ants is equal to the number of endpoints and the ants are placed at the positions of the endpoints

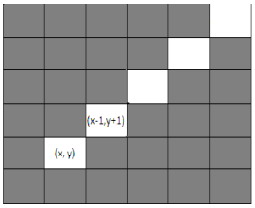

Fig.3 End point pixel (x,y)[16].

Following transition rule of has been used to find the next pixel position:

Transition rule: The transition rule takes into account the probability of undetected edge pixels only. For the ant movement, the probability factor for eight neighbouring pixels is calculated using probability transition matrix according to Eq. (1). The pixel with maximum probability factor of the undetected neighbouring pixels is included in the set of edge pixels.

To reduce the redundant movement of ants the stopping rules proposed in [16] has been implemented. These rules are shown in the Fig. 4.

Rule 1) The movement of the ant is stopped when it touches the track already traversed by another ant.

Rule 2) When all the neighboring pixels (8 pixels in 3*3 grid) are already traversed by the ant, then the movement of ant stops.

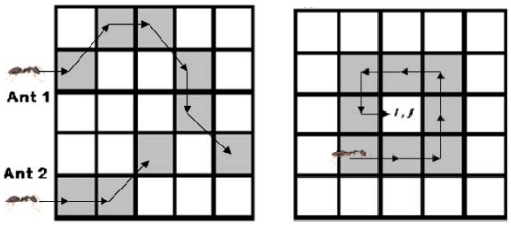

Fig.4 Ant's movement representing rule(1) and (2)[16]

3.3 The Ant Colony Algorithm for Edge Improvement

The ACO algorithm is used to increase the connectivity of the edges in the image obtained after applying local adaptive thresholding. The steps are as follows:

1) Initialize the ant's position by placing them only at end points.

2) Initialise the pheromone matrix and calculate the heuristic information using Eq.(2)

3) Construction Process:

For the ant index 1 : k

Move the k^{th} ant for L steps according to the probabilistic transition matrix using Eq. (1)

4) Calculate maximum probability of transition as per the t*ransition rule* and move the ant accordingly.

5) Perform local pheromone update process using Eq. (3)

6) Check whether all ants have moved one step, if yes, perform the global pheromone update using Eq. (4).

7) Check whether the ant can move to the next position by applying the stopping rules, if not, stop the ant.

8) Decision Process:

The pheromone matrix so produced is used to extract the complete edge trace by applying thresholding.

9) The edge pixels obtained are combined with the edge pixels obtained by adaptive thresholding to get the complete edge information.

The flow chart of the proposed algorithm is shown in Fig. 5.

IV. RESULTS AND DISCUSSION

4.1 Comparison with other techniques

This section presents the experimental results of the proposed technique against traditional edge detectors such as Canny, Edison, Prewitt, Sobel and Susan. In these experiments, traditional edge detectors are executed by MATLAB toolbox. The codes for our method were also written in MATLAB. The results were obtained using the following values of parameters: $\alpha = 0.5$ $and \beta$=1. The edge pixels are colored white on a black background.

Fig.5. Shows the original images used for experiments. The Fig. 6(a)-(e) to 8 (a)-(e) shows the output after application of different edge detectors, Fig. 6(f) to 8(f) shows the output after adaptive thresholding, Fig 6(g) to 8(g) shows the output of ACO and Fig. 6(h) to 8(h) shows the output of the proposed method. The default values (which gives the best edge map) of the thresholding is selected while using the MATLAB function directly for the edge detectors. It can be seen that the more connected edge map is obtained by the proposed method. For example in Lena image the edge pixels pointed as A, B, C and D have not been detected by any other edge detectors. The proposed algorithm results in more edge pixels with reduced noise. Above discussion shows that the proposed method performs well as compared to other conventional edge detectors. It provides more edge information with noise reduced to a greater extent.

4.2 Shanon's Entropy

The performance of most of the edge detectors proposed in the literature is visually analyzed. Sometimes the visual analysis is insufficient to prove that the proposed method gives more connected edges. To overcome this problem we use the entropy function for quantitative analysis.

The information content of the output image is measured by using Shannon's entropy function. It gives the indefiniteness in an image and is calculated as:

$$H(I) = -\sum_{i=0}^{n} p_i \log p_i \qquad (6)$$

where, I stand for image whose entropy is to be measured. p_i is the frequency of pixels with intensity I. Table 1 shows the

entropy values for various edge detectors. Higher the value of entropy higher will be the information content. However, a very large value of entropy shows larger noise content or double edges.

The Canny edge detectors produce double edges and SUSAN method produces a larger noise content, therefore the entropy value obtained using this two methods is higher as compared to the proposed method. The other edge detector namely Sobel, Prewitt and Edition gives the less edge information; therefore the entropy values obtained using these methods are less than the proposed method.

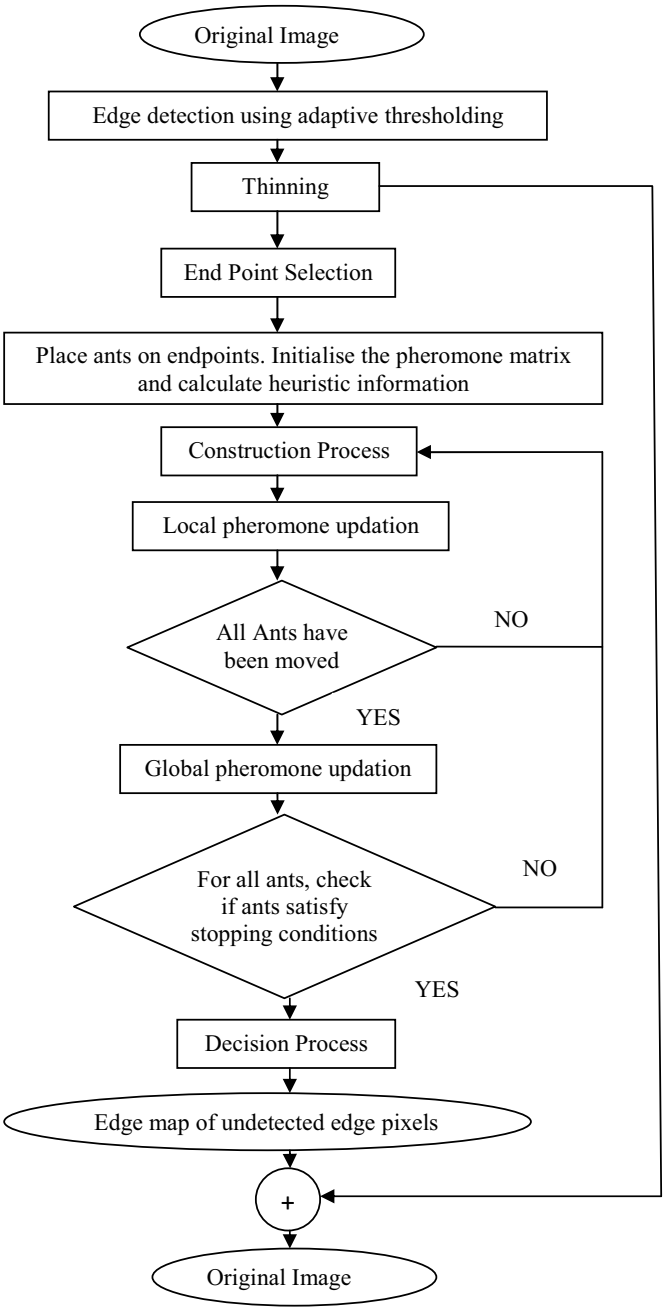

Fig.5 Flowchart for proposed algorithm

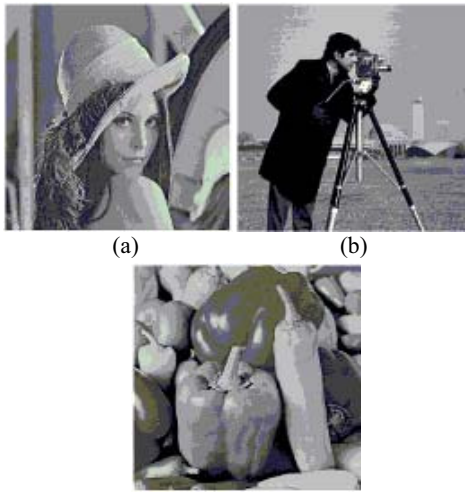

Figure 5 Original Images (a) Lena (b) Cameraman (c) Peppers.

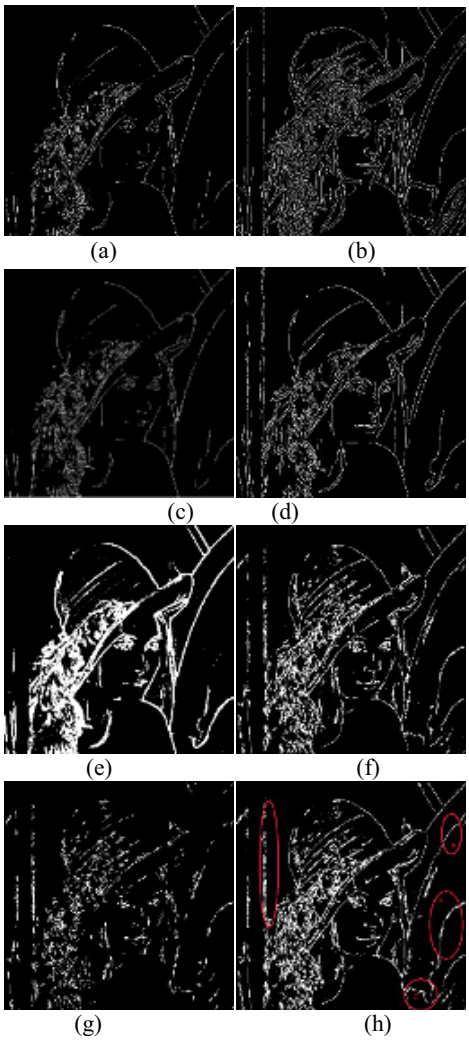

Figure 6. Edge map using (a) Sobel (b) Canny (c) Prewitt (d) Edison (e) SUSAN (f) Adaptive (g) ACO (h) Proposed.

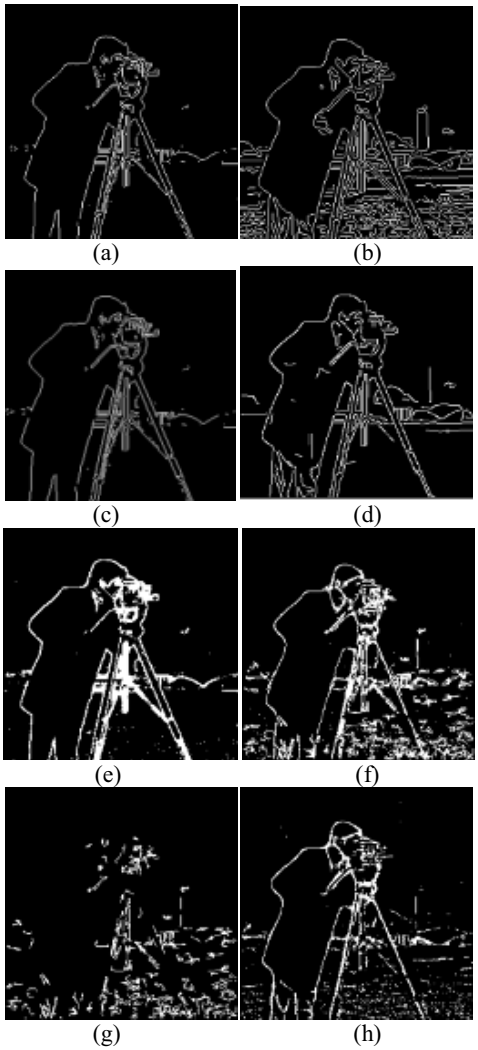

Figure 7. Edge map using (a) Sobel (b) Canny (c) Prewitt (d) Edison (e) SUSAN (f) Adaptive (g) ACO (h) Proposed.

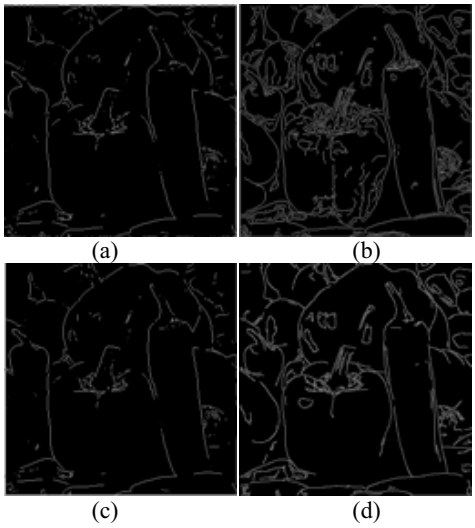

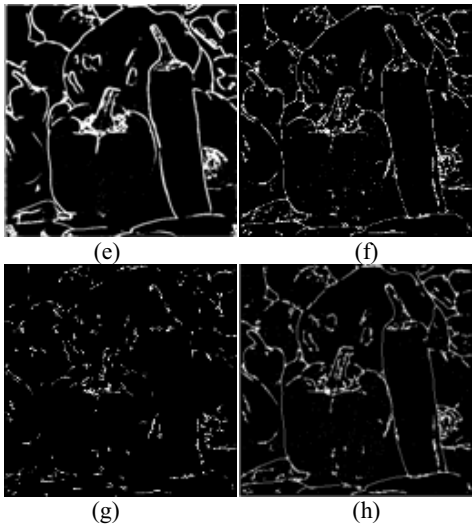

Figure 8. Edge map using (a)Sobel (b)Canny (c)Prewitt (d)Edison (e) SUSAN (f)Adaptive (g)ACO (h)Proposed

4.3 Effect of parameter variation

In most of the application of ACO the selection of the two parameters namely α *and* β, affects the results. We examine the effect of these parameters on entropy value calculated for a test image (Lena). This effect is illustrated in Fig 9 and Fig 10. It is shown that entropy value is almost constant with the variation over a large range of these parameters.

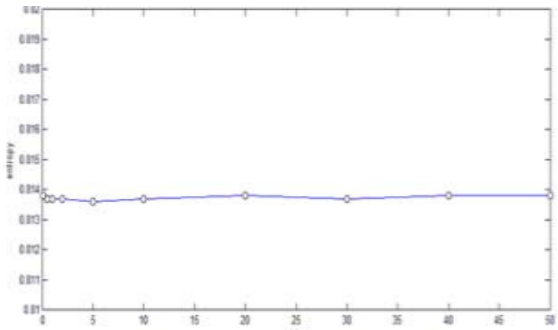

Figure 9. Variation of entropy with alpha

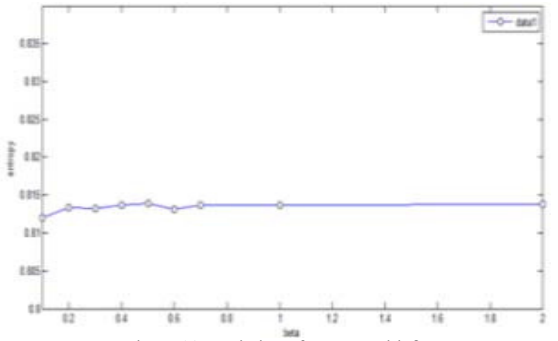

Figure 10. Variation of entropy with β

Table I Entropy values for different edge detectors

Image\Method	Sobel	Prewitt	Edison	Susan	Canny	Proposed
Lena	0.5314	0.5247	0.6774	1.05	0.8866	0.8137
Cameraman	0.5633	0.5629	0.6852	1.4081	0.9931	0.8013
House	0.4483	0.4447	0.8085	1.12	0.7354	0.6677
Pepper	0.3596	0.3493	0.6184	0.8894	0.7846	0.6837

V. CONCLUSIONS

Adaptive thresholding and ACO based image edge detection has been undertaken in this study. The adaptive thresholding is used for edge detection and ACO is used for edge improvement. The ants in the proposed study move on the edge pixels undetected by the adaptive thresholding method. This reduces the redundant edge pixels and results in more connected edges. For the qualitative analysis of the proposed method over the traditional edge detectors, the results are analyzed using Shannon's Entropy function. The edge detection through adaptive thresholding provides larger end points information as compared to traditional edge detector, therefore in the proposed study edges extracted from adaptive thresholding is preferred over the traditional edge detectors.

REFERENCES

[1] Gonzales, R.C., Woods, R.E., 2002. *Digital Image Processing*.Prentice Hall.

[2] Canny JF.,"A computational approach to edge detection" *IEEE Trans Pattern Anal Mach Intell*1986;8(6):679–98.

[3] Marr, D., and Hildreth, E.C., "Theory of edge detection",*Proc. of the Royal Society of London*,vol 207, 1980,pp 187-217.

[4] S.M.Smith and J.M.Brady ,"SUSAN- A new approach to low level image processing",,*International Journal of Computer Vision23*(1) 1997, pg 45-78.

[5] Parker, J.R., 1997. Algorithms for Image Processing and Computer Vision ,*Wiley Computer Publication.*

[6] Ng, C.M., Leung, W.L., Lau, F., "Edge detection using evolutionary algorithms", In: *IEEE Internat. Conf. on System,Man and Cybernetics,Tokyo,Japan,* 12th-15th October 1999, pp. 865–868.

[7] Sharifi, M., Fathy, M., Mahmoudi, M.T., "A classified and comparative study of edge detection algorithms", In: *IEEE Proc. Internat. Conf. on Information Technology: Coding and Computing,* 8th-10th April 2002, pp. 117–120.

[8] Marco Dorigo, Thomas Stutzle "From Real to Artificial ants", MIT Press Book, ISBN0262042193, 2004.

[9] M. Dorigo, M. Birattari, and T. Stutzle, "Ant colony otimization," *IEEE Computational Intelligence Magazine,* vol. 1, pp. 28–39, Nov. 2006.

[10] M. Dorigo V. Maniezzo and A. Coloni, "Ant system: Optimization by a colony of cooperation agents", *IEEE Trans on System Man and Cybernetics*, Part B, Vol. 26, pp 29-41, Feb 1996.

[11] M. Dorigo and L.M. Gambardella,"Ant Colony System:" A cooperative learning approach to the travelling salesman problem." *IEEE Trans*. On Evolutionary Computation, Vol 1,Number 1, pp.53-61.April 1997.

[12] T. Stutzle and H. Holger H, "Max-Min ant system", *Future Generation Computer Systems,* vol. 16, pp. 889–914, Jun. 2000.

[13] Li Hong, ZiongShibo, " On Ant Colony Algorithm for solving Continuous Optimization Problem", *IEEE International Conference on Intelligent Information Hiding and Multimedia Signal Processing, Harbin USA*,15-17 August 2008, pp 1450-1453.

[14] Jingan Yang, YanbinZhuang, "An Improved ant colony optimization algorithm for solving a complex combinatorial optimization problem", *Applied Soft Computing*, Volume 10 ,Issue 2: March 2010.

[15] Hossein Nezamabadi-pour, Saeid Saryazdi, EsmatRashedi, "Edge detection using ant algorithms", *Soft Computing*, 2006, Number 6, Vol 10: Pg:623–628.

[16] O.P. Verma, M. Hanmandlu, Ashish Kumar Sultania, Dhruv "A Novel Fuzzy Ant System for Edge Detection", Computer and Information Science, *IEEE/ACIS 9th International Conference, Yamgata Japan,*18th-20th August 2010 , Page(s): 228 – 233.

[17] Das. Lu, C.C. Chen, "Edge Detection improvement by ant colony optimization", *Pattern Recognition Letters* Vol 29, Issue 4, 2008, pp 416-425.

[18] Jian Zhang, Kun He, Jiliu Zhou, Mei Gong, "Ant colony optimization and statistical estimation approach to image edge detection", *WiCOM, Chengdu,China* , 23th-25th September 2010 ,IEEE, Page(s): 1 – 4.

[19] Jevtić, A., Andina, D. "Adaptive Artificial Ant Colonies for Edge Detection in Digital Images", *IECON,Glendale, AZ, USA*, 7th-10th November 2010, IEEE, Page(s): 2813 – 2816.

[20] O.P. Verma, M. Hanmandlu, P. Kumar, and A. Jindal, "A Novel Bacterial Foraging Technique for Edge Detection", *Pattern Recognition Letters* Vol. 32, pp. 1187–1196, 2011.

[21] N. Otsu "A Threshold Selection method from gray level histograms", *IEEE Trans.Syst.,Man,Cybern*,Vol 9,pp 62-66,Jan 1979.

[22] O.P. Verma, M. Hanmandlu, Punit Kumar, Shivangi Shrivastava "A novel approach for edge detection using ant colony optimization and fuzzy derivative technique", *Advance Computing Conference, 2009.IEEE international, Patiala India*, 6th-7th March 2009 page(s):1206 – 1212

[23] Sergey Subbotin and Alexey Oleynik, "Modifications of Ant Colony Optimization Method for Feature Selection*", CADSM'2007*, 20th-24th February, 2007, Polyana, UKRAINE.

[24] Xiang Ming, Wu XiaopeiHuaQuanping, "A Fast Thinning Algorithm for Fingerprint Image", *The 1st International Conference on Information Science and* Engineering (ICISE2009),Nanjing, China,18th-20th December 2009.

MATERIALS CHARACTERIZATION XX (2012) XXX–XXX

Available online at www.sciencedirect.com

SciVerse ScienceDirect

www.elsevier.com/locate/matchar

Nanocrystalline non-stoichiometric SBT: Effect of milling duration on structural and electrical characteristics

Sugandha[a], A.K. Jha[a,b,*]

[a]Thin Film and Material Science Laboratory, Department of Applied Physics, Delhi Technological University (Formerly Delhi College of Engineering), Delhi-110042, India

[b]Department of Applied Sciences, Ambedkar Institute of Technology, GGSIPU, Geeta Colony, Delhi-110092, India

ARTICLE DATA

Article history:
Received 28 August 2011
Received in revised form
14 December 2011
Accepted 23 December 2011

Keywords:
Electro-ceramics
Nanocrystalline SBT
Dielectric property

ABSTRACT

In the present work, nanocrystalline specimens of non-stoichiometric Strontium Bismuth Tantalate (SBT) ferroelectric ceramics were synthesized by mechanical activation process using a high energy planetary ball mill. The powders were milled for different milling durations (5, 10, 20 h) keeping the milling speed fixed at 300 rpm. Microstructural characterizations have been performed using X-ray diffraction, scanning electron microscopy, electron diffraction and transmission electron microscopy. Nanocrystallites with average grain size in the range of 30–50 nm are observed to be formed. Grain size is observed to decrease with increasing milling duration. Detailed dielectric study as a function of temperature has been carried out. It is observed that dielectric constant increases and dielectric loss decreases with increasing milling duration. The observed characteristics have been explained in terms of increased number of grain boundaries due to the reduction of granular size.

1. Introduction

Nanocrystalline ferroelectric ceramics are important electronic materials having a wide range of scientific and industrial applications such as high dielectric constant capacitors, piezoelectric transducers, pyroelectric sensors, non volatile ferroelectric random access memories, etc. It is well known that performance of any material is closely related to its synthesis process. The methods of synthesis of ferroelectric powders play a significant role in determining the microstructural, electrical and optical properties of these materials [1–3]. Conventionally these ceramics are synthesized by solid state reaction process, using constituent oxides/carbonates as the starting materials. In the last decades, various wet chemistry methods such as chemical co-precipitation, sol–gel, hydrothermal synthesis [4–6], etc. have also been explored to synthesize nanocrystalline ferroelectric ceramics. Although significant progress has been achieved, there are certain problems associated with above techniques. For example, sol–gel process uses metal alkoxides as the starting material which are very expensive and extremely sensitive to the environmental conditions such as moisture, light and heat. Co-precipitation technique involves repeated washing in order to eliminate anions coming from the precursor salts used, making the process complicated and time consuming. Furthermore, it is difficult to produce large batches by using most of the chemical solution processing routes. Therefore, exploring alternative methods for the preparation of ferroelectric ceramics is still of scientific and technological significance.

Mechanical activation (high energy ball milling) is a technique which has been recently used to synthesize various ferroelectric ceramics such as $PbZr_{1-x}Ti_xO_3$ (PZT), $BaTiO_3$, $Ba_5SmTi_3Nb_7O_{30}$ and various bismuth containing aurivillius

* *Corresponding author at:* Department of Applied Sciences, Ambedkar Institute of Technology, GGSIPU, Geeta Colony, Delhi-110092, India. Tel.: +91 98 68 24 21 50; fax: +91 11 27 87 10 23.
E-mail addresses: miglani.sugandha@gmail.com (Sugandha), Prof.akjha@gmail.com (A.K. Jha).

1044-5803/$ – see front matter © 2012 Published by Elsevier Inc.
doi:10.1016/j.matchar.2011.12.011

compounds such as $Bi_4Ti_3O_{12}$ (BiT), $SrBi_2Ta_2O_9$ (SBT), $SrBi_4Ti_4O_{15}$, etc. [7–10]. The most significant characteristic of this technique is the formation of the desired compound is due to the reaction of the oxide precursors which are activated by mechanical energy, instead of the heat energy required in conventional solid state reaction technique. Secondly, it takes place at room temperature in well sealed containers, thus effectively minimizing the loss of the volatile components such as lead and bismuth.

It is worth mentioning here that in the mechanical activation technique, milling duration has significant effect on the phase formation and final particle/grain size in the synthesized specimens. Excessive milling is known to introduce various defects such as contamination, lattice distortion, stress, vacancies, etc. Elimination of these defects takes place at the expense of grain growth [11]. Therefore, in this procedure it is possible to control the final particle/grain size of synthesized specimen by optimizing the milling duration. As discussed earlier, mechanical activation technique is a promising technique for the synthesis of bismuth layer structured ferroelectric ceramics. This is due to the fact that this technique does not require high temperature calcination and lowers the sintering temperature, which is the main drawback in the conventional solid state reaction technique.

Among bismuth layer structured ferroelectrics, stoichiometric SBT has generated great interest due to its promising properties such as high dielectric constant, high remnant polarization, low dielectric loss, low leakage current, etc [12]. However, due to bismuth volatilization, stoichiometric SBT suffers from many intrinsic defects such as oxygen vacancies. This results in degraded ferroelectric properties and fatigue endurance [13,14]. It has been reported that by varying Sr/Bi ratio in starting composition comparatively enhanced electrical properties are obtained at lower processing temperature [15,16]. The lack of reports in mechanically activated non-stoichiometric SBT has prompted the authors to synthesize $Sr_{0.8}Bi_{2.2}Ta_2O_9$ compound by varying the milling duration and investigate its effects on the structural and electrical properties.

2. Experimental Procedure

Highly pure powders of $SrCO_3$, Bi_2O_3, Ta_2O_5 (all from M/s Aldrich) were mixed to yield $Sr_{0.8}Bi_{2.2}Ta_2O_9$. This mixture of powders was milled in a high-energy planetary ball mill (Retsch, PM 100) for 5, 10, and 20 h at a milling speed of 300 rpm. Milling was carried out in toluene medium with a high wear-resistant 10 mm zirconium oxide balls in a zirconium oxide vial with a ball-to-powder weight ratio of 10:1. The mixture was then admixed with 2 wt.% polyvinyl alcohol as a binder and then pressed at 200 MPa into a disk shaped pellet. These pellets were then sintered at 1100 °C for 2 h in air on alumina crucibles.

Phase development in the synthesized compound was monitored using an X-ray diffractometer (Bruker, D8 Advance) with CuK_α radiation ($\lambda = 1.5405$ Å) at a scanning rate of 1°/min. Transmission electron microscopy (Jeol, 2100-F) and scanning electron microscopy (Hitachi, S-3700N) were used to study their structural morphology. The sintered pellets were polished and silver pasted on both sides and cured at 500 °C for 1 h. The dielectric measurements were carried out using a precision LCR meter (Agilent 4284A) at an oscillation amplitude of 1 V. The dc electrical resistivities of the samples were measured using a programmable electrometer (Kiethley, 6517A).

3. Results and Discussions

3.1. Structural and Microstructural Studies

Fig. 1 compares the X-ray diffraction (XRD) patterns of the $Sr_{0.8}Bi_{2.2}Ta_2O_9$ powders milled for different durations i.e. 5, 10, and 20 h. The XRD peaks were indexed using the observed d-values and software package, Powder X [17]. It can be seen that phase development starts from 5 h and improves with the duration of milling. A shift of the peaks toward higher angles is seen on increasing the milling duration. The specimen milled for 20 h clearly exhibit layered perovskite phase formation with distinct (115), (008), (200) and (220) peaks. Further, the broadening of the characteristic peaks such as (115), (006), (220), etc. indicates the reduction of particle size and the formation of nanocrystallites in the specimen milled for 20 h. When the specimen is milled for longer duration like 20 h using zirconium balls and vial, it is likely that some zirconium atoms enter the perovskite structure [18]. However, no

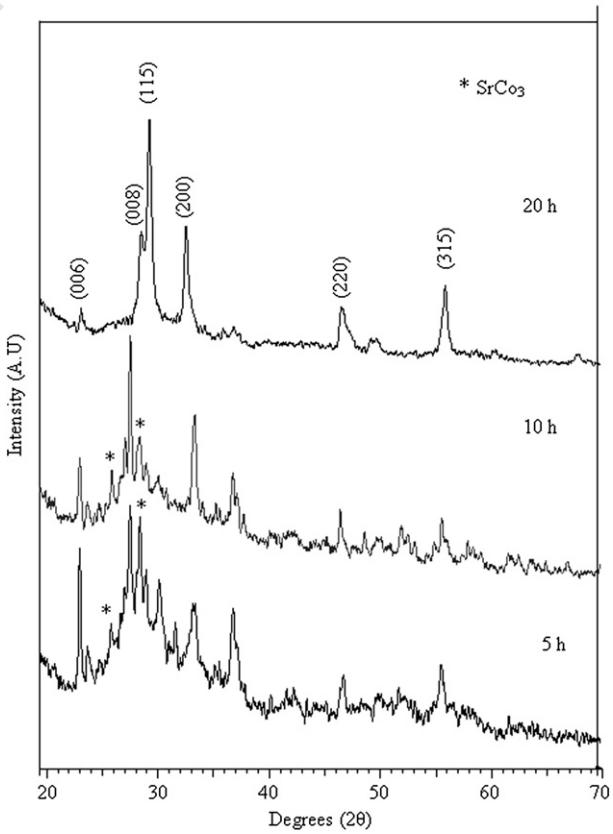

Fig. 1 – X-ray diffraction patterns of $Sr_{0.8}Bi_{2.2}Ta_2O_9$ powders subjected to different milling durations of mechanical activation process.

Please cite this article as: Sugandha , Jha AK, Nanocrystalline non-stoichiometric SBT: Effect of milling duration on structural and electrical characteristics, Mater Charact (2012), doi:10.1016/j.matchar.2011.12.011

such extra peaks corresponding to ZrO_2 or the compound involving zirconium are seen in the XRD diffractograms. Further, had zirconium entered the structure during the milling process the peak should have shifted to lower angles instead of the observed shift towards higher angles as the ionic radii of Zr^{4+} (0.79 Å) is higher that that of Ta^{5+} (0.64 Å). This is possibly due to high wear resistant balls and vials used in the present work [19,20].

Fig. 2 shows the scanning electron microscope images of the specimen milled for different durations. The size of the particles is seen to be decreasing with increasing milling time. It is observed that the sample milled for 5 h exhibit large particles with many small size grains are seen to stick to the surface of large grains. In the specimen milled for 10 h, the number of large particles gets reduced forming loose agglomerate. The sample milled for 20 h shows a dense microstructure indicating agglomeration of particles due to further reduction in the grain size. The images obtained from transmission electron microscopy and electron diffraction of the studied specimen milled for 20 h are shown in Fig. 3. The average particle size is seen to be in the range of 30–50 nm. Also, the formation of particles of nano dimensions is further confirmed by the appearance of diffraction rings consisting of discrete diffraction spots in the electron diffraction pattern. As shown in the diffraction pattern, five distinct rings have been indexed [21,22]. The phase formation of ferroelectric nanocrystallite specimen using high energy ball milling is a complex process. Mechanical activation of starting oxides/carbonates, to form desired ferroelectric phase, takes place in two stages. In the first stage, the milling process reduces the particle size of the starting oxides. This results in the formation of high defect densities, shorter diffusion distances, more intimate contacts of precursors, etc. At the

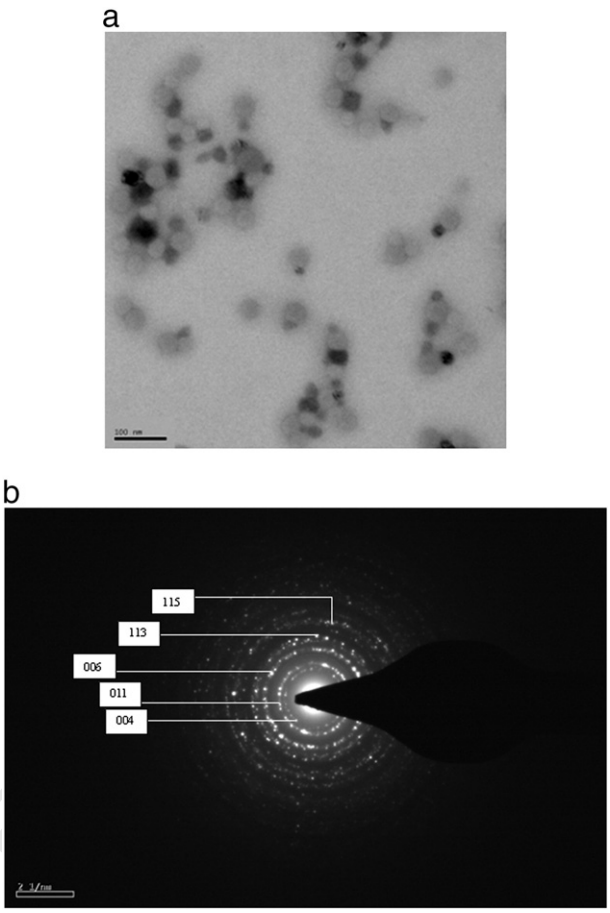

Fig. 3 – Transmission electron micrograph and electron diffraction pattern of 20 h milled $Sr_{0.8}Bi_{2.2}Ta_2O_9$ powder.

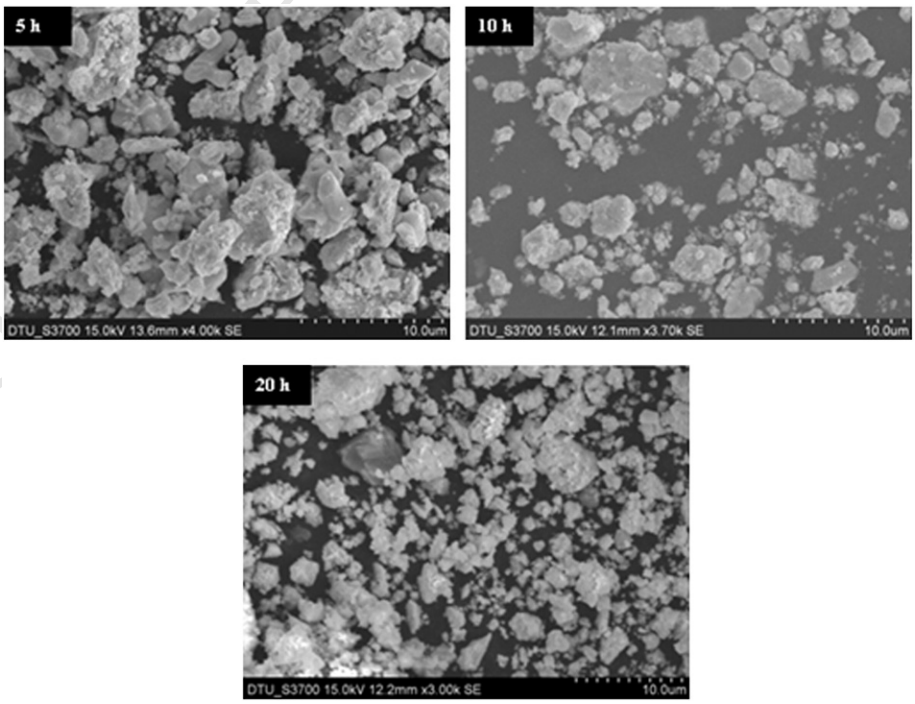

Q3 **Fig. 2 – Scanning electron micrographs of $Sr_{0.8}Bi_{2.2}Ta_2O_9$ powders prepared at different milling durations.**

Please cite this article as: Sugandha , Jha AK, Nanocrystalline non-stoichiometric SBT: Effect of milling duration on structural and electrical characteristics, Mater Charact (2012), doi:10.1016/j.matchar.2011.12.011

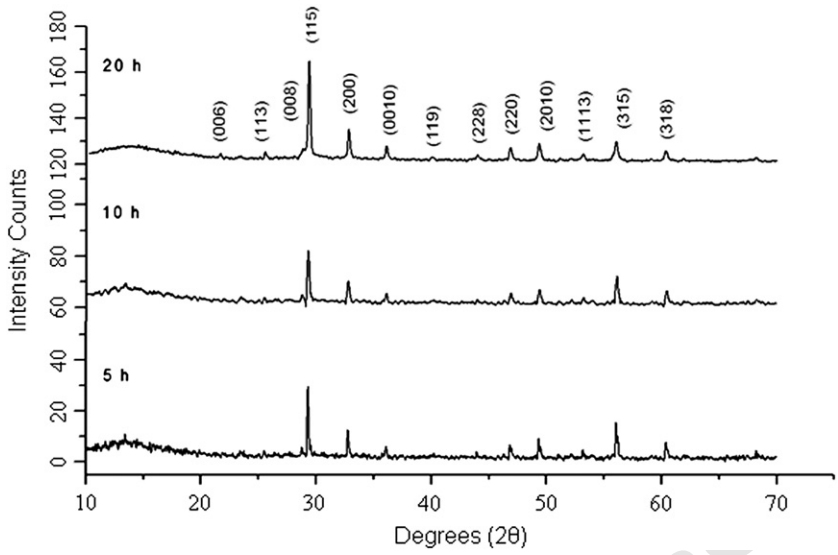

Fig. 4 – X-ray diffraction pattern of $Sr_{0.8}Bi_{2.2}Ta_2O_9$ sintered samples milled at different durations.

same time fresh/cleansed surface interfaces are also created. All these factors contribute to enhance the reactivity and sinterability of the starting oxide mixture. In the later stage, after sufficient activation, nucleation and growth of the nanocrystallite structure takes place resulting into the formation of desired perovskite ferroelectric phase. This is attributed to the

Table 1 – Comparison of different parameters in $Sr_{0.8}Bi_{2.2}Ta_2O_9$ samples prepared by mechanical activation process for different milling durations.

Milling duration (h)	a (Å)	b (Å)	c (Å)	V (Å^3)	Crystallite size (nm)	ε_{max}	T_c (K)
5	5.4772	5.5089	24.8451	749.659	60.8	578.532	653
10	5.4719	5.5058	24.7021	742.168	39	759.786	643
20	5.4573	5.5027	24.6451	740.089	27.6	859.325	628

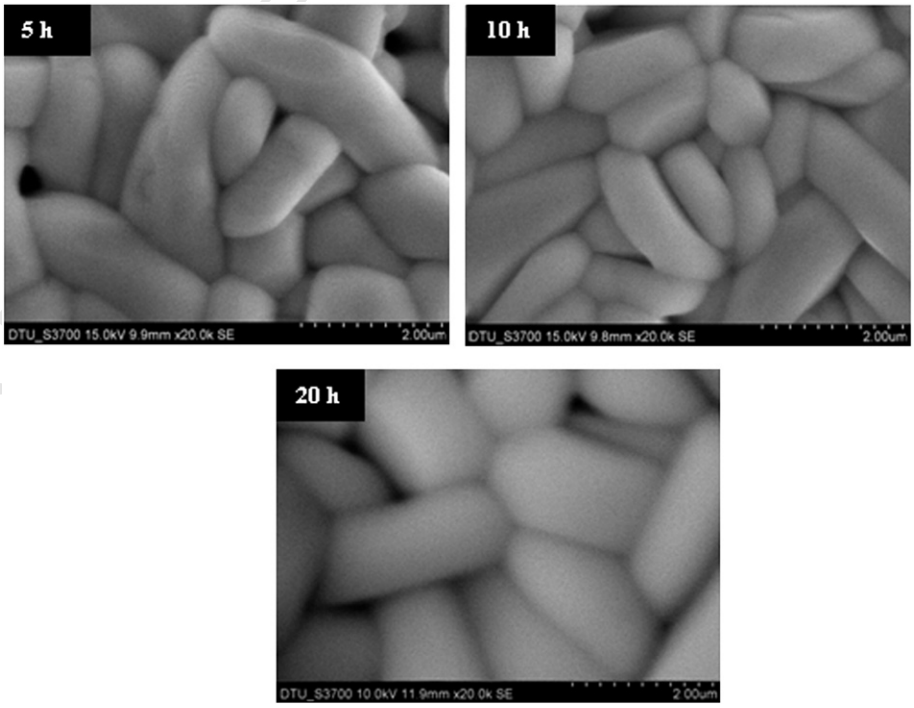

Fig. 5 – Scanning electron micrographs of $Sr_{0.8}Bi_{2.2}Ta_2O_9$ sintered samples milled at different durations.

Please cite this article as: Sugandha , Jha AK, Nanocrystalline non-stoichiometric SBT: Effect of milling duration on structural and electrical characteristics, Mater Charact (2012), doi:10.1016/j.matchar.2011.12.011

local heating and high localized pressure during collision of zirconium balls with the vial. It is worth mentioning here that although the overall temperature of a milling system is lower than 100 °C, the "in situ" impact temperature is sufficiently high to activate the solid state reaction [23,24].

Fig. 4 shows the X-ray diffractogram patterns of the sintered specimen milled for different durations. It is observed that single phase layered perovskite structure is formed in all the samples. In these diffractograms the shift of peaks to slightly higher angles with increasing milling duration is observed. It was observed that the d-values of the characteristic peaks are matching with that obtained in the X-ray diffractogram patterns (Fig. 1) of the as-milled powders suggesting the initiation of the development of the layered perovskite phase in the milled powders. The lattice parameters for the synthesized samples were calculated using the observed interplanar spacing, d-values, obtained from the diffractograms and refined using the least square refinement method by the computer program package Powder X are given in Table 1. It is observed that the lattice parameters and unit cell volume decrease with increase in milling duration. The crystallite size calculated from the broadening of X-ray diffractogram peaks using the Scherrer's formula [25] of milled $Sr_{0.8}Bi_{2.2}Ta_2O_9$ decreases with increasing milling time (Table 1). The corresponding scanning electron micrographs of the sample prepared at different milling times are shown in Fig. 5. The average grain size of the sintered specimen decreases from 1 to 2 μm in the sample milled for 5 and 10 h to <1 μm in the sample milled for 20 h. Also, the calculated surface area increases from 22 m^2/g in the sample milled for 5 h to 28 m^2/g and 43 m^2/g respectively in the samples milled for 10 and 20 h.

3.2. *Dielectric Studies*

The temperature dependence of dielectric constant (ε'_r) and dielectric loss (tanδ) measured at 100 kHz are shown in

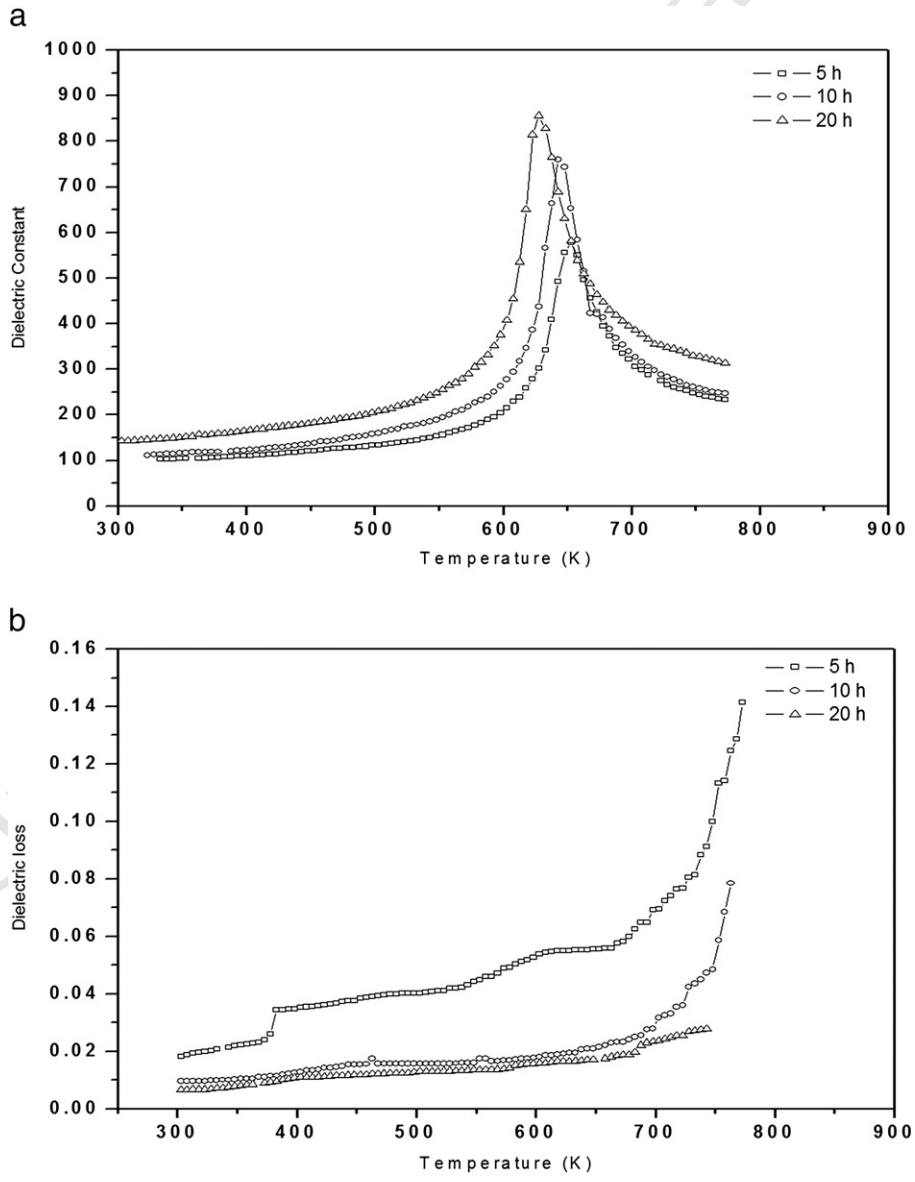

Fig. 6 – Temperature variation of (a) dielectric constant (ε'_r) and (b) dielectric loss (tanδ) for mechanical activation processed samples at different milling durations.

Please cite this article as: Sugandha , Jha AK, Nanocrystalline non-stoichiometric SBT: Effect of milling duration on structural and electrical characteristics, Mater Charact (2012), doi:10.1016/j.matchar.2011.12.011

Fig. 6(a) and (b) for all the studied samples. All the samples exhibit sharp ferroelectric to paraelectric phase transition at their respective Curie temperature (T_c). It is observed in Fig. 6(a) that dielectric constant value increases with increase in milling time and is maximum in the sample milled for 20 h. Further, Curie temperature is observed to decrease with increase in milling duration (Table 1). It is known that in the fine grained specimen, the dielectric constant increases due to an increase in residual internal stress [26–28]. Thus, the increase in ε'_r value can be attributed to the decrease in the average grain size with an increase in milling time (Fig. 5). The observed decrease in transition temperature with increasing milling time is attributed to the reduction in grain size [29,30]. It is known that specimens with smaller grains posses more interfacial or grain boundary energy as it contains larger number of grain boundaries. This results in the requirement of smaller amount of thermal energy to undergo the phase transition resulting in the reduction of T_c [31].

Fig. 6(b) shows the variation of dielectric loss (tanδ) as a function of temperature for all the studied samples. It is observed that dielectric loss decreases with increasing milling duration and is minimum in the sample milled for 20 h. This is possibly due to improved and dense mirostructure having less porosity (as observed in Fig. 5) [32,33]. In all the samples it is observed that tanδ remains nearly constant in the lower temperature region and thereafter increases rapidly at higher temperature. However, the loss in the sample milled for 20 h does not considerably increase in higher temperature region. The sharp increase of dielectric loss at high temperature region can be attributed to the increased mobility of space charges arising from defects or vacancies (oxygen vacancies) in the sample [34].

3.3. *D.C. Conductivity*

Fig. 7 shows the variation of dc conductivity ($\sigma_{dc}=1/\rho$) with inverse of temperature ($10^3/T$) of the studied specimens. For all the studied samples, conductivity is constant in the lower temperature region and thereafter increases considerably with temperature. This indicates negative temperature coefficient of resistance (NTCR) type behavior. As seen in the figure, there are two predominant types of conduction mechanism, one is the lower temperature region in which dc conductivity remains invariant with temperature and the other is higher temperature region in which dc conductivity increases sharply with temperature. In lower temperature region from room temperature to approximately ~573 K the electrical conduction is dominated by extrinsic defects such as unintentionally added impurities. Whereas, in higher temperature region ~573 K to ~973 K the conduction is dominated by intrinsic defects [35,36]. It is observed that dc conductivity decreases with milling duration and is lowest for 20 h milled sample. This can be attributed to the increase in scattering of charge carriers. It is known that various types of defects such as grain boundaries, pores, vacant spaces, etc. affect the motion of charge carriers [37]. In nanocrystalline specimens, scattering by grain boundaries is more pronounced as compared to scattering by defects or impurities. This is due to the fact that nanocrystalline samples have high grain boundary area to volume ratio resulting into an increase in electron scattering. Therefore, the sample milled for 20 h exhibit lower electrical conductivity as compared to the samples milled for 5 and 10 h [38].

4. Conclusion

Nanocrystalline $Sr_{0.8}Bi_{2.2}Ta_2O_9$ has been successfully synthesized by the mechanical activation process. The synthesized samples exhibit single phase layered perovskite structure. Transmission electron microscope image and electron diffraction patterns reveal that the particle size in the specimen milled for 20 h reduces to nano range. As the milling duration has increased dielectric constant increases considerably whereas the Curie temperature decreases slightly. $Sr_{0.8}Bi_{2.2}Ta_2O_9$ compound

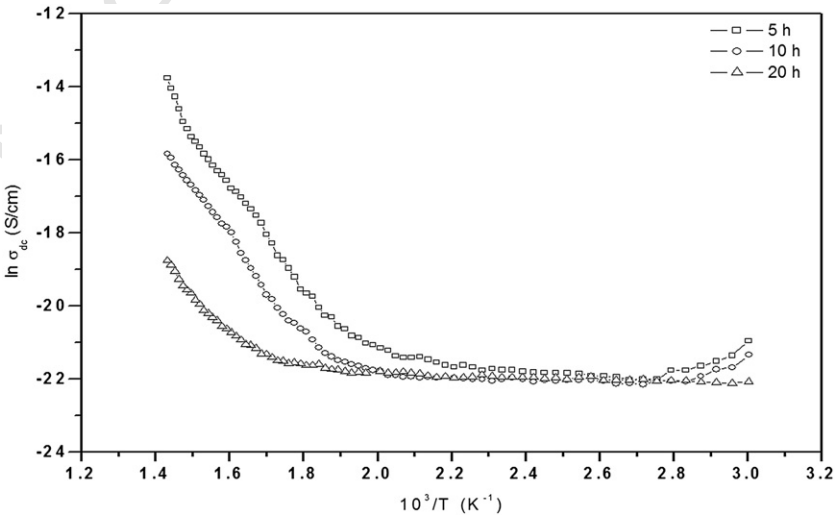

Fig. 7 – Variation of dc conductivity ($\ln\sigma_{dc}$) with inverse of temperature ($10^3/T$) for mechanical activation processed samples at different milling durations.

Please cite this article as: Sugandha , Jha AK, Nanocrystalline non-stoichiometric SBT: Effect of milling duration on structural and electrical characteristics, Mater Charact (2012), doi:10.1016/j.matchar.2011.12.011

prepared by above technique for 20 h milling exhibit highest dielectric constant, dc resistivity and lowest dielectric loss.

Acknowledgment

Authors expressed their thanks to UGC, New Delhi for the research grant (Grant No-F. No. 39-469/2010 (SR)).

REFERENCES

[1] Kiezer K, Janssen EH, Burggraaf AJ. Influence of particle size and structure of ZrO_2 on microstructure development and dielectric constant of Pb $(Zr_{0.5}Ti_{0.5})O_3$. Mater Res Bull 1973;8:533–44.
[2] Yamamoto T. Optimum preparation methods for piezoelectric ceramics and their evalution. Am Ceram Soc Bull 1992;71:978–85.
[3] Arlt G. The influence of microstructure on the properties of ferroelectric ceramics. Ferroelectrics 1990;104:217–27.
[4] Camargo ER, Frantti J, Kakihana M. Low-temperature chemical synthesis of lead zirconate titanate (PZT) powders free from halides and organics. J Mater Chem 2001;11:1875–9.
[5] Kim S, Jun M, Hwang S. Preparation of undoped lead titanate ceramics via sol–gel processing. J Am Ceram Soc 1999;82:289–96.
[6] Sato S, Murakata T, Yanagi H, Miyasaka F. Hydrothermal synthesis of fine perovskite $PbTiO_3$ powder with a simple mode of size distribution. J Mater Sci 1994;29:5657–63.
[7] Ganguly P, Jha AK. Enhanced characteristics of $Ba_5SmTi_3Nb_7O_{30}$ ferroelectric nanocrystalline ceramic prepared by mechanical activation process: a comparative study. Mater Res Bull 2011, doi:10.1016/j.materresbull.2011.01.016.
[8] Xue JM, Wang T, Toh W. Synthesis of lead zirconate titanate from an amorphous precursor by mechanical activation. J Alloys Compd 2000;308:139–46.
[9] kong LB, Ma J, Zhu W, Tan OK. Preparation of $Bi_4Ti_3O_{12}$ ceramics via a high-energy ball milling process. Mater Lett 2001;51:108–14.
[10] Sritharan T, Boey FYC, Srinivas A. Synthesis of complex ceramics by mechanochemical activation. J Mater Process Technol 2007;192:255–8.
[11] Kong LB, Zhang TS, Ma J, Boey F. Progress in synthesis of ferroelectric ceramic materials via high energy mechanochemical technique. Prog Mater Sci 2008;53:207–322.
[12] Coondoo I, Jha AK. Effect of sintering temperature on the structural, dielectric and ferroelectric properties of tungsten substituted SBT ceramics. Physica B 2011;406:374–81.
[13] Araujo CAP, Chuchiaro JD, Mcmillan LD, Scott MC, Scott JF. Fatigue-free ferroelectric capacitors with platinum electrodes. Nature (London) 1995;374:627.
[14] Zuong Y, Hu G, Tang T. Preparation and ferroelectric properties of lanthanum modified $Sr_{0.8}Bi_{2.2}Ta_2O_9$ thin films. Jpn J Appl Phys 2003;42(1):7424–7.
[15] Noguchi T, Hase T, Myasaka M. Analysis of the dependence of ferroelectric properties of strontium bismuth tantalate thin films on the composition and process temperature. Jpn J Appl Phys 1996;35:4900 [Part1].
[16] Atsuki T, Soyama N, Yonezawa T, Ogi K. Preparation of Bi-based ferroelectric thin films by sol–gel method. Jpn J Appl Phys 1995;34:5096.
[17] Dong C. Powder X: windows-95-based program for powder X-ray diffraction data processing. J Appl Crystallogr 1999;32:838.
[18] Jiang JZ, Poulsen FW, Morup S. Structure and thermal stability of nanostructured iron-doped zirconia prepared by high energy ball milling. J Mater Res 1999;14:1343–52.
[19] James AR, Subrahmanyam J. Processing and structure–property relation of fine-grained PLZT ceramics derived from mechanochemical synthesis. J Mater Sci Mater Electron 2006;17(7):529–35.
[20] Beitollahi A, Moravej M. Phase formation study of PZT nanopowder by mechanical activation method at various conditions. J Mater Sci 2004;39(16, 17):5201–7.
[21] Williams DB, Carter CB. Transmission electron microscopy – a textbook for materials science – second part. New York: Plenum Press; 1996.
[22] Andrews K, Dyson D, Keown S. Interpretation of electron diffraction patterns. New York: Plenum Press; 1971.
[23] Xue JM, Wan DM, Lee SE, Wang J. Mechanochemical synthesis of lead zirconate titanate from mixed oxides. J Am Ceram Soc 1999;82(7):1687–92.
[24] Takacs L. Multiple combustion induced by ball milling. Appl Phys Lett 1996;69:436–8.
[25] Scherrer P. Estimation of the size and internal structure of colloidal particles by means of Roëntgen. Gott Nachr 1918;2:98–100.
[26] Buessem WR, Cross LE, Goswami AK. Phenomenological theory of high permittivity in fine-grained barium titanate. J Am Ceram Soc 1966;49(1):33–6.
[27] Arlt G, Henning D, de With G. Dielectric properties of fine-grained barium titanate ceramics. J Appl Phys 1985;58(4):1619–25.
[28] Uchino K, Sadanaga E, Hirose T. Dependence of the crystal structure on particle size in barium titanate. J Am Ceram Soc 1989;72(8):1555–8.
[29] Parashar SKS, Choudhary RNP, Murthy BS. Ferroelectric phase transition in $Pb_{0.92}Gd_{0.08}(Zr_{0.53}Ti_{0.47})_{0.98}O_3$ nanoceramic synthesized by high-energy ball milling. J Appl Phys 2003;94(9):6091–6.
[30] Parashar SKS, Choudhary RNP, Murthy BS. Size effect of $Pb_{0.92}Nd_{0.08}(Zr_{0.53}Ti_{0.47})_{0.98}O_3$ nanoceramic synthesized by high-energy ball milling. J Appl Phys 2005;98:104305.
[31] Callister WD. Material science and engineering: an introduction. India: Wiley; 2006.
[32] Huang YN, Wang YN, Shen HM. Internal friction and dielectric loss related to domain walls. Phys Rev B 1992;46:3290.
[33] Su B, Holmes JE, Cheng BL, Button TW. Processing effects on the microstructure and dielectric properties of barium strontium titanate (BST) ceramics. J Electroceram 2002;9:111–6.
[34] Ganguly P, Jha AK. Enhancement of dielectric properties by optimization of sintering condition in tungsten–bronze structured $Ba_5SmTi_3Nb_7O_{30}$ ferroelectric ceramics. J Electroceram 2009;22:257–62.
[35] Dhak D, Dhak P, Pramanik P. Influence of substitution on dielectric an impedence spectroscopy of $Sr_{1-x}Bi_{2+y}Ta_2O_9$ ferroelectric ceramics synthesized by chemical route. Appl Surf Sci 2008;254:3078–92.
[36] Shulman HS, Testorf M, Damjanovic D, Setter N. Microstructure, electrical conductivity, and piezoelectric properties of bismuth titanate. J Am Ceram Soc 1996;79:3124.
[37] Poole CP. Introduction to nanotechnology. New Jersey: Wiley Interscience; 2003. p. 232.
[38] Ashby MF. Nano-materials, Nanotechnology &Designs; 2000. p. 219.

Please cite this article as: Sugandha , Jha AK, Nanocrystalline non-stoichiometric SBT: Effect of milling duration on structural and electrical characteristics, Mater Charact (2012), doi:10.1016/j.matchar.2011.12.011

giftjourn@l
Global Journal of
Flexible Systems Management
2011, Vol. 12, Nos. 1 & 2, pp 81-89

Performance Optimization of an Imbalanced Flexible Manufacturing System Using Taguchi Approach

Ravindra Kumar
Mechanical & Automation Engineering Department, GPM College of Engineering, Delhi. India
E-mail address: ravi3000@gmail.com

Abid Haleem
Mechanical Engineering Department, Jamia Millia Islamia, Delhi. India

Suresh K. Garg
Production & Industrial Engineering Department, Delhi Technological University, Delhi. India

Rajesh K. Singh
Indian Institute of Foreign Trade, Delhi. India

Abstract

Considering the diverse range of manufacturing capabilities of modern manufacturing systems, uniform distribution of load on the workstations (WSs) is difficult to achieve as some of the WSs are required to process more parts than others or sometimes processing time of a WS can differ from one part to the other. These situations lead to unbalancing of the manufacturing system. The objective of this paper is to study and optimize the performance of an imbalanced Flexible Manufacturing System (FMS) under different operating environments. The FMS under consideration manufactures three types of parts having different processing characteristics. The experimental variables for the study are buffer capacities at the WSs, reduction in processing time of bottleneck WS, WSs processing time distribution, and parts release control. Throughput, average work-in-process (AWIP) and Average Throughput Time (ATT) are taken as performance measures.

Taguchi approach is used to analyze the effects of above variables and establish the combinations of best factor levels to get the optimal performance. All variables are found to affect the performance to some extent. Reduction in processing time of the bottleneck WS and processing time distribution affected the performance of the system severely. The best factor level combinations differ for parts having different processing characteristics. This paper may help industry in analyzing the performance of an imbalanced FMS.

Keywords: bottleneck, buffer capacity, imbalanced flexible manufacturing system, parts release control, taguchi, workstation

Introduction

Increased global competition attracted the business leaders and policy makers to turn their attention towards productivity and quality issues. In the present competitive scenario, manufacturing industries are facing great challenges for their survival. In the modern manufacturing environment, FMSs have evolved to meet the globalized market challenges. The particular characteristic of FMS is its capacity to operate effectively and efficiently under the changing market and technological production conditions (Angelo *et al.*, 1996). Gupta and Buzacott (1989) observed that there is no uniformly agreed definition of the term FMS. According to Stockton and Bateman (1995), flexibility is the ability of a manufacturing system to change quickly and economically between existing part types, operation routes of components, operations on a component, production volumes, and capability to add new part types and new processes to the system. The flexibility is gained at the expense of a complex control system required to control the processing workstations and the material handling system.

FMS is an integration of Computerized Numerical Control (CNC) machines and a material handling system. The three primary parts of the system are CNC machine centers with automated tool changes, a material handling system and a mainframe computer to control the overall system. According to Klahorst (1981), FMS is a group of machines and related equipments brought together to process a group or family of parts and includes some primary and secondary components for a complete FMS. Ranky (1983) has defined an FMS as a system dealing with high level distributed data processing and automated material flow using computer-controlled machines, assembly cells, industrial robots, inspection machines and so on, together with computer integrated material-handling and storage systems. Meredith (1989) has been defined FMS as “a group of machines and related equipments brought together to

completely process a group or family of parts". Lee (2007) has defined FMS as a group of material processing cells connected by an automated material handling system to manufacture a low to medium volume of a wide variety of products.

The most commonly used material handling systems in FMS are Automated Guided Vehicles (AGVs), conveyors, and industrial robots. In modern manufacturing environments, AGV systems have become an integral part of overall manufacturing systems (Aized, 2009). Buffer is also an important element of any manufacturing system which improves the performance by storing the parts temporarily at the WSs thereby reducing the idle time of WSs due to the non availability of parts. In general the advantage of high buffer capacity causing high utilization is offset by the disadvantage of additional floor space and inventory (Saad and Byrne, 1998). It is known that higher buffer capacities are better; however, one important question arises at what level of buffer capacities, the benefit of increased buffer size cease to justify the buffer space investment required.

The most commonly used material handling systems in FMS are Automated Guided Vehicles (AGVs), conveyors, and industrial robots.

A number of WSs are used in FMS depending on the types of parts processed and the number of operations performed on these parts. Some of the WSs are required to perform more number of operations than others. Therefore all WSs are not uniformly loaded. When the workload on the WSs is not uniformly distributed i.e. a few may be critically loaded while others are loaded partially, then the system is called an imbalanced manufacturing system. An imbalanced manufacturing system tends to have underutilized operators and workstations along with high work in process (Chow, 1988).

The remaining part of the paper is organized as follows: Section 2 presents the literature review, in section 3 FMS configuration has been described, section 4 presents the assumptions made in the study. In section 5 results have been presented and section 6 concludes this paper.

Literature Review

The stiff competition and demanding customers forced the industries to shift from mass production to mass customization. Hence, the manufacturers are concentrating to such type of production technologies in which changes can be made with minimum possible time and cost to produce small batches to unit products. This needs to incorporate flexibility in their manufacturing system. Many authors have classified the flexibility considering the likely changes required according to the future trends of the market and technological advancements. One of the classifications is provided by describing nine types of flexibilities (Browne *et al.,* 1984). These are machine flexibility, process flexibility, product flexibility, routing flexibility, routing flexibility, volume flexibility, expansion flexibility, process sequence flexibility, and production flexibility.

The stiff competition and demanding customers forced the industries to shift from mass production to mass customization.

In an imbalanced FMS some of the WSs are underutilized due to the bottlenecking of parts flow through the overloaded WS. An imbalance measure is some function of workload differences among WSs (Kumar and Shankar, 2001). In both conventional and flexible manufacturing systems, workload balancing attempts to equalize the workload of the operations assigned to each WS (Farkas *et al.*, 1999). A simulation study was carried out by Monch *et al.*, (2001) to solve the load balancing problems for the photolithography area of wafer fabrication in a semiconductor fabrication facility. By Hayrinen *et al.* (1998) the jobs were allocated initially in the first phase and then tuned to a balanced WS allocation in the next phase. With unbalanced workload scenarios a periodic steady state without non-productive time has obviously been reached by the bottleneck workstations only. In fact, on the other workstations, non-productive times are always present and cannot be eliminated (Cardarelli and Pelagagge, 1992).

Many authors have worked on balancing the work load on the workstations. Rajakumar *et al.* (2004 & 2007) have worked through the sequencing rule and genetic algorithm for minimizing the workload imbalance in parallel machines. Raghavendra and Murthy (2010) have developed two strategies in the pre-release and planning stages to reduce the imbalance between the parallel machines. They have also proposed a genetic algorithm based heuristic approach minimizing the imbalance of workload among the identical parallel machines (Raghavendra and Murthy, 2011). Biswas and Mahapatra (2009) have a meta-heuristic approach based on particle swarm optimization to solve the machine loading problem in FMS. Shafiq et. al. (2010) studied the effects of routing flexibility and analyzed that routing flexibility improve the performance with small penalty on processing time but deteriorate in case of larger penalties. Ali and Wadhwa (2010) studied the routing flexibility in FMS involving variety production for minimizing the make-span as a performance by integrating different entities flowing in the system. Ali *et al.* (2010) considered a real industrial problem to analyze the impact of routing flexibility which improved the performance of the system.

Buffer is another vital issue in a manufacturing system. It can be shown that the buffer capacity is a very important design parameter for any system and it is very clear that the selection of buffer capacities has a significant effect on the performance (Saad and Byrne, 1998). The studies also have shown that the performance is more sensitive at low levels of buffer capacity than at higher levels, (El-rayah, 1979, Shafiq et. al., 2010). A limited buffer capacity in both input and output places of workstations gives the possibility for the system to experience a deadlock situation where no

material can move (Caumond *et al.*, 2009). Kim *et al.*, (1997) suggested the following measures for the deadlock avoidance of the system:

- Flow-shop design (the machines are laid out in a unidirectional flow pattern).
- Stations with large buffers.
- Limited numbers of jobs in the system.

Another strategy for deadlock-free design is to use a central storage area. All jobs pass through this area before going to the working station. Chan and Chan (2004) evaluated the performance of an FMS under different routing strategies in addition with the infinite and finite local buffer capacities and shown that a particular routing strategy outperforms other strategies if the local buffer size is infinity. It is also shown that no particular dispatching rule performs well in all buffer sizes and infinite buffer size is not the best choice in all the cases.

Kosturiak and Gregor (1998), have shown that Load Oriented Control (LOC) and Drum Buffer Rope (DBR) type of parts release controls into the manufacturing system improve all the system parameters considerably and allow finding a reasonable compromise between the high system utilization and the short throughput times and low inventories. They also studied that this control principles allow the reduction of the buffers and the simplification of the whole control and monitoring system in the production. The implementation of the DBR control is easier in comparison with the LOC because it is sufficient to control only the inventory level on the bottlenecks in the production for this concept.

Traditionally, the FMS problems have been solved by analytical methods but computer simulation method has gained popularity as it enables to model the complex manufacturing systems.

Traditionally, the FMS problems have been solved by analytical methods but computer simulation method has gained popularity as it enables to model the complex manufacturing systems. This method has the capabilities like statistics collection, real time observation, animation and dynamic adjustability (Tunali, 1996). The simulation models have been developed using general purpose programming languages (C, FORTRAN, PASCAL, etc.), general simulation languages (GPSS, SLAM, SIMSCRIPT, etc.) special purpose simulation packages (WITNESS, SEE-WHY, SIMFACTORY, etc.) (Goyal *et al.* 1995).

Denzler *et al.* (1987) performed an analysis of scheduling rules with machine breakdown and variable performance times for a dedicated FMS using simulation. Yildirim, *et al.* (2006) used artificial neural network to analyze the performance of FMS when utilizing only a portion of the available capacity by decreasing the number of workers or halting production on some of the WSs/production lines while preserving the flexibility of production system to satisfy demand spikes. Pramod and Garg (2006) observed that most of the research in the area of FMS has been carried out at the initial level of developing concept regarding flexibility, uncertainty and performance of the system.

Ali et al. (2010) considered a real industrial problem to analyze the impact of routing flexibility which improved the performance of the system.

From the above literature it can be concluded that only a few studies include the optimization of imbalanced FMS in context of performance variables such as buffers capacity, improvement in bottleneck WS, processing time distribution and parts release control.

FMS Configuration

Figure 1 shows an FMS model layout used in this study which is a modification of the model used by Kosturiak and Gregor (1998). This FMS consists of six workstations (WSs) distanced 15 meters apart, on which three types of parts P1, P2 and P3 with processing times shown in Table 1, are processed. To take the issue of mass customization this FMS has product mix flexibility and assumed to be capable of processing a mixed part types in different proportions depending on the availability of processing WSs for the above three part types. The FMS also has the production flexibility which enables it to process the families of parts whose processing time variation follows Erlang and normal distribution within the family.

The FMS considered for this study is highly imbalanced i.e. the WSs are loaded unevenly. Some of the WSs are critically loaded while others are loaded partially. Bottleneck WS processing time is taken so as to match with the parts arrival rate. The parts arrive at the input storage of the system from where these can be released according to a predetermined rule.

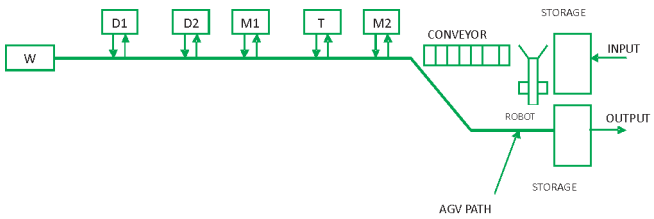

Figure 1: FMS Layout (Kosturiak and Gregor, 1998)

D1, D2 – Drilling Machines 1 and 2

M1, M2 – Milling Machines 1 and 2

T – Turning Machine

W – Washing Machine

Robot handling time – 2.5 min

Conveyor total time to transfer a part – 2.8 min

AGV speed 30 m/min

AGV load/unload time – 30 sec

Table 1: Parts Processing Plan

Part Types	First Arrival (min)	Time Between Arrivals (min)	Processing Time					
			D1	D2	M1 (Bottleneck WS)	M2	W	T
P1	0	50	40	21	-	-	15	12
P2	23	69	-	-	34.5	14	15	12
P3	46	69	-	-	34.5	-	15	12
Machine Total Load →			40	21	69	14	45	36

FMS Variables

FMS variables are the factors which affect the performance of the system. The following variables have been considered in the present study:

Buffer Capacities at the WSs

In the present study three cases of buffer capacities have been considered; all buffers incapacitated, buffers at the bottleneck WS incapacitated and others with a capacity of 10, and all buffers with a capacity of 10.

Processing Time of Bottleneck WS

Bottleneck WS is the crucial element of any manufacturing system. It causes the traffic congestion and delays the flow of parts to other WS thereby reducing the performance of the system. The performance of the system can be improved by the percentage reduction in processing time of the bottleneck WS (Angelo *et al.* 1996). Here, three levels of bottleneck WS's processing times i.e. 34.5, 31, and 27.5 min (approximately 10% reduction in processing time) have been considered.

Processing Time Distribution

The processing time of the WSs is one of the important aspects which contribute to the performance of the system. As FMS is used for manufacturing mixed parts of a group or family of parts in which the processing time changes from one part to another within the family, therefore the processing time within the families can be considered to vary as fourth order Erlang distribution (Sabuncuoglu and Hommertzheim 1992, Ross *et al.*, 1996). The Erlang distribution is chosen over the exponential distribution since an FMS generally processes a more homogeneous population of parts (Ross *et al.* 1996). To account for the variation in processing time three levels of processing times distribution have been considered; deterministic, Erlang distribution, and normal distribution.

Parts Release Control

Limited buffer capacity at the input/output ends of WSs makes the possibility for the deadlock situation where parts movement is held completely. To avoid collisions and deadlock situation in a manufacturing system parts release is controlled according to some predefined rule. In the present study, two cases of parts release control have been considered i.e. Load Oriented Control (LOC) and Drum Buffer Rope (DBR) control. In LOC type of control, a production order is not released into the system if it exceeds the load limit of a WS by at least one of its operations. Here, the parts are released from the store if all the buffers have parts less than the specified limit. In the DBR type of control, parts are released from the store into the system if the buffer at the bottleneck WS has parts less than the specified limit irrespective of the parts at other WSs. In this study three cases of parts release controls have been considered; no control i.e. parts are released as and when they arrive, load oriented control (LOC) i.e. parts released when parts in all the buffers are less than 10, and drum buffer rope (DBR) controls i.e. parts released when parts in buffer at bottleneck WS are less than 10.

Bottleneck WS is the crucial element of any manufacturing system.

Performance Measures

The following performance measures have been considered for evaluating the effect of above variables:

- **Throughput:** Throughput is taken as the number of each part type manufactured during the total simulation period of one week.
- **Average Work-in-Process (AWIP):** This is the average of work-in-process during the total simulation period.
- **Average Throughput Time (ATT):** This is the average time taken by each part for processing through the system.

The performance of the system can be improved by the percentage reduction in processing time of the bottleneck WS (Angelo et al. 1996)

Assumptions of the Proposed FMS Study

Several assumptions have been made in order to evaluate the performance of the system under the given operating conditions. These also include assumptions from Sabuncuoglu and Hommertzheim's (1992) study. The assumptions are:

- Each WS handles one operation at a time.
- Machine setup time is included in the operation time.
- Separate buffers are available at the input/output ends of the WSs.
- Incapacitated buffer means it has large storage capacity.

- Material pallets and tooling are not considered as constraints.
- AGVs carry one part at a time.
- AGVs are continuously operational without any breakdown.
- Two separate parallel tracks are assumed for up and down motion of the AGVs.
- The AWIP and ATT are considered from the arrival of the parts in the input storage to the shipment of part.
- FIFO rule is used for scheduling of parts.

To avoid collisions and deadlock situation in a manufacturing system parts release is controlled according to some predefined rule.

Results and Discussions

Kosturiak and Gregor (1998) studied the influence of various control strategies on the FMS parameters and evaluated the effects of improvement in performance of the FMS with the improvement of machines. In this paper the effects of improving the performance of bottleneck WS, buffer capacities, processing time distribution and parts release controls have been evaluated. The simulation model was developed using the WITNESS simulation software from Lanner Group. WITNESS is one of the simulation software for simulating the automated manufacturing systems. In this software a manufacturing system is modeled using available design elements. After modeling next step is to detail the various elements of the system. Detailing is the logical relationship between these design elements of the manufacturing system. Once all the elements of the system have been detailed the model can be run and the various activities can be viewed on the screen in the form of graphics. Thereafter the statistics report can be viewed in the form of tables and charts. The performance parameters of the system can be studied by changing the design variables in manufacturing system. The system with the best performance is chosen. In the present study to evaluate the performance under different operating conditions the FMS was initially simulated for a warm up period of one week i.e. 10080 min (7 x 24 x 60) and data collected for a period of next one week. As it would have not been possible to analyze the effects of each variable in combination with other variables i.e. full factorial design, therefore Taguchi method is applied to analyze the interactions among the variables.

WITNESS is one of the simulation software for simulating the automated manufacturing systems.

Taguchi Experiment

Taguchi method is a form of design of experiment with the application of reduced number of experiments. Taguchi method is a technique for designing and performing experiments where many factors affect the performance of the system. The approach of Taguchi method is shown in Figure 2. It uses a statistical measure of performance called signal-to-noise (S/N) ratio which are used to measure the effect of noise factors on the performance characteristics. S/N ratios take into account the mean closeness to the target and the range of variability in the response data. The S/N ratio can be expressed in terms of performance measure such as for AWIP as follows:

$$\text{S/N ratio } (\beta) = -10 \log_{10} (\text{AWIP})^2$$

There are several S/N ratios available depending on the type of characteristics but the following three of them are considered standard (Bryne and Taguchi, 1986; Phadke, 1989):

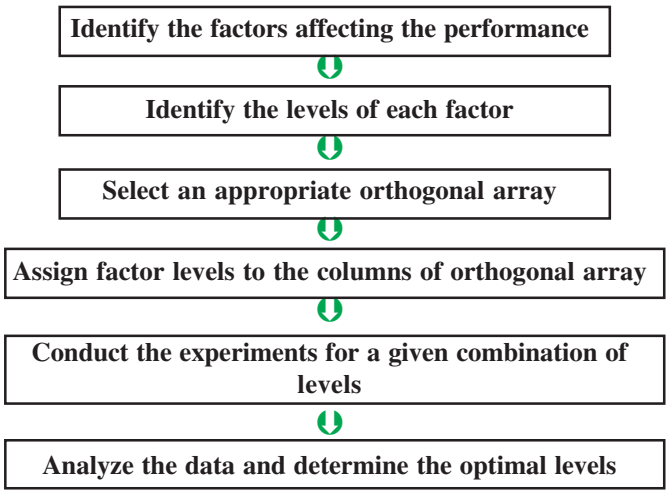

Figure 2: Taguchi Method Approach

- Smaller is better
- Larger is better
- Nominal is better

In the present case the performance values AWIP and ATT follow the first standard i.e. smaller is better.

Matrix Experiment Simulation Results

In the present study considering the numbers of factors and their levels, an orthogonal array (L9) consisting of nine experiments has been selected. The combination of different levels is shown in table 2. The experiments are performed for the above combinations of factor levels and data presented in table 3. From the data it is observed that there is negligible effect of different factor levels on the throughput but AWIP and ATT changes significantly. Hence, optimization is performed for AWIP and ATT through Taguchi experimental framework involving analysis of means (ANOM) and analysis of variance (ANOVA). The S/N ratios account for these two values which are used to identify the optimal factor combinations generating the best system performance and analyzing the relative significance of factors contributing to the AWIP and ATT.

Analysis of Results

The objective of performing the matrix experiment is to identify the optimum factor combinations. The main effect of a factor is the deviation caused from the overall mean.

Table 2: Factor Level Details

Factor	Level	Value
Buffer Capacity (BFC)	A1	All incapacitated
	A2	BWS-Incapacitated, Others-10
	A3	All-10
BWS Processing Time (BWS_PT)	B1	34.5 min
	B2	31 min
	B3	27.5 min
Processing Time Distribution (PTD)	C1	Deterministic
	C2	Erlang Distribution
	C3	Normal Distribution
Parts Release Control (PRC)	D1	No Control
	D2	LOC (Parts released when all buffers have parts less than 10)
	D3	DBR (Parts released when buffer at BWS has parts less than 10)

The main factor effects are estimated using the following:

$$M_{jk} = \frac{\sum_{l=1}^{l} B\,jkl}{l}$$

Where:

M_{jk} = main effect value of factor j at the k^{th} level.

B_{jki} = S/N ratio of factor j with level k.

The graphical representations of main effects of different factor levels are shown in Figures 3 and 4. From the graphs it is observed that bottleneck WS processing time affects the AWIP and ATT significantly for parts which are processed on the bottleneck WS but the effects are negligible on part P1. The processing time distribution of WSs also affects the AWIP and ATT significantly in the same proportion for all the parts. Buffer capacities at the WSs affect the performance to some extent. In case of buffer capacity levels 2 and 3 i.e. limited buffer capacities at the WSs the performance improves in respect of parts P2 and P3. It is also observed that parts release control lowers the performance of the system in respect of part P1 but remain unaffected for parts

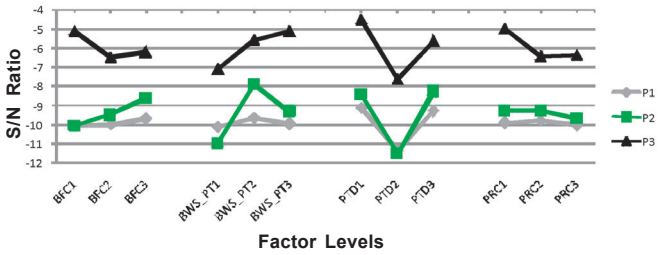

Figure 3: Effects of Each Factor Level on AWIP

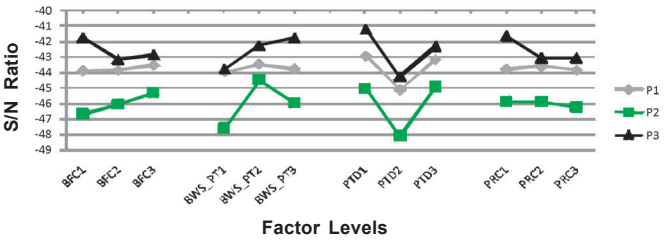

Figure 4: Effects of Each Factor Level on ATT

P2 and P3 in case of LOC type of control however for DBR type of control the performance deteriorates.

The best factor level combinations are listed in Table 5. It is observed that a combination of smaller buffer capacities at the WSs, approximately 10 % reduction in bottleneck WS processing time, deterministic processing time, and LOC type of control give best performance in respect of part P1 and P2. However, the best combination for part P3 is different. The different factor level combinations are due to the different processing conditions for each part and needs to be evaluated for the best combination.

Conclusions and Scope of Future Research

In the present study, the performance of an imbalanced FMS has been analyzed. The simulation method is used to find the effects of different variables on the performance of the FMS. Taguchi approach has been used to reduce the number of experiments. S/N ratios which account for the analysis of means and deviation in performance are used rather than the direct output of the system. The variables considered for the study have a significant impact on the performance of the

Table 3: Matrix Experiment Factor Levels and Simulation Results

Expt. No.	FACTORS				Throughput (Parts)			AWIP (Parts)			ATT (min)		
	A	B	C	D	P1	P2	P3	P1	P2	P3	P1	P2	P3
1.	A1	B1	C1	D1	202	145	147	2.97	3.36	1.58	145.85	228.77	107.36
2.	A1	B2	C2	D2	204	143	146	3.59	3.36	2.23	175.86	227.06	150.64
3.	A1	B3	C3	D3	202	145	146	3.02	2.87	1.67	148.71	195.41	114.02
4.	A2	B1	C2	D3	202	145	143	3.87	4.72	3.08	189.19	315.05	211.03
5.	A2	B2	C3	D1	201	147	146	2.85	2.18	1.76	141.0	147.8	120.13
6.	A2	B3	C1	D2	202	146	146	2.86	2.59	1.73	140.44	176.53	117.49
7.	A3	B1	C3	D2	202	145	147	2.88	2.81	2.41	141.76	191.29	162.93
8.	A3	B2	C1	D3	203	147	146	2.74	2.1	1.76	133.95	142.21	119.86
9.	A3	B3	C2	D1	201	145	148	3.64	3.36	2.04	178.32	228.6	137.85

Table 4: Factor Main Effects Values

Factor Level Main Effect	Applicable Formula	Main effect value AWIP			Main effect value ATT		
		P1	P2	P3	P1	P2	P3
M_{A1}	$(\beta_1+\beta_2+\beta_3)/3$	-10.0524	-10.0704	-5.13119	-43.8761	-46.7099	-41.7718
M_{A2}	$(\beta_4+\beta_5+\beta_6)/3$	-9.9928	-9.5047	-6.48073	-43.8241	-46.0991	-43.1600
M_{A3}	$(\beta_4+\beta_5+\beta_6)/3$	-9.7216	-8.6484	-6.24773	-43.5313	-45.2913	-42.8672
M_{B1}	$(\beta_1+\beta_4+\beta_7)/3$	-10.1234	-10.9933	-7.12817	-43.9491	-47.5965	-43.7813
M_{B2}	$(\beta_2+\beta_5+\beta_8)/3$	-9.6513	-7.9134	-5.59553	-43.4755	-44.5250	-42.2418
M_{B3}	$(\beta_3+\beta_6+\beta_9)/3$	-9.9832	-9.3168	-5.13595	-43.8069	-45.9789	-41.7759
M_{C1}	$(\beta_1+\beta_6+\beta_8)/3$	-9.1125	-8.4124	-4.54811	-42.9223	-45.0610	-41.1968
M_{C2}	$(\beta_2+\beta_4+\beta_9)/3$	-11.3594	-11.5108	-7.64324	-45.1551	-48.0906	-44.2779
M_{C3}	$(\beta_3+\beta_5+\beta_7)/3$	-9.2950	-8.3003	-5.66831	-43.1541	-44.9488	-42.3242
M_{D1}	$(\beta_1+\beta_5+\beta_9)/3$	-9.9247	-9.27423	-5.02533	-43.7622	-45.9210	-41.660
M_{D2}	$(\beta_2+\beta_6+\beta_7)/3$	-9.8057	-9.25564	-6.45579	-43.6281	-45.8977	-43.0663
M_{D3}	$(\beta_3+\beta_4+\beta_8)/3$	-10.0365	-9.69362	-6.37853	-43.8412	-46.2817	-43.0667

Table 5: Best Factor Level Combination for Different Performance Measures

Best Factor Level Combination for Different Performance Measures						
Level	AWIP			ATT		
	P1	P2	P3	P1	P2	P3
Buffer Capacity	A3	A3	A1	A3	A3	A1
BWS-PT	B2	B2	B3	B2	B2	B3
PTD	C1	C1	C1	C1	C3	C1
PRC	D2	D2	D1	D2	D2	D1

system. Throughput of the system has not been affected to the considerable level as input rate is in consistence with the processing rate of bottleneck WS. Irrespective of throughput, a significant impact on AWIP and ATT is observed.

It is observed that some of the variables have relatively more impact on the performance than the others. The degree of impact also depends on the processing characteristics of the part type i.e. part processed or not processed on the bottleneck WS, part having smaller/larger total processing time. The impact of buffer capacities shows that larger buffers do not add values always and even can deteriorate the performance. Impact of parts processing time distribution show that processing of families of parts (processing time changes from part to part within the family) also affects the performance severely. The combinations of best factor levels have been established. These combinations found to differ for parts having different processing characteristics.

This study has been limited to optimize an imbalanced FMS in context of buffer capacity, improved bottleneck WS, parts processing time distribution, and parts release control. The future work can be extended to a wide range of levels. Other variables such as alternate routing of parts from the bottleneck WS, AGVs quantity and speed, machine break down, distance between WSs, scheduling rules can be included for further study of an imbalanced FMS.

References

Aized T. (2009). Modelling and Performance Maximization of an Integrated Automated Guided Vehicle System Using Coloured Petri Net and Response Surface Methods. *Computers and Industrial Engineering,* 57:822-831.

Ali, M. and Wadhwa S. (2010). The Effect of Routing Flexibility on a Flexible System of Integrated Manufacturing. *International Journal of Production Research,* 48(19):5691-5709.

Ali M., Salahuddin and Khan M.A. (2010). Analysis of the Impact of Routing Flexibility on the Performance of Flexible System. *International Journal of Industrial Engineering,* 17(4):269-278.

Angelo A.D., Gastaldi M. and Levialdi N. (1996). Dynamic Analysis of the Performance of a Flexible Manufacturing System: A Real Case Application. *Computer Integrated Manufacturing Systems,* 9:101-110.

Biswas S., Mahapatra S.S. (2009). An Improved Meta-Heuristic Approach for Solving the Machine Loading Problem in Flexible Manufacturing Systems. *International Journal of Services and Operations Management,* 5(1):76-93.

Browne J., Dubois D., Rathmill K., Sethi S. P. and Stecke K.E. (1984). Classification of Flexible Manufacturing Systems. *The FMS Magazine,* pp. 114-117.

Bryne D.M. and Taguchi S. (1986). The Taguchi Approach to Parameter Design. ASQC Quality Congress Transactions, Anaheim, CA, pp. 168.

Cardarelli G. and Pelagagge P.M. (1992). FMS Control Rule Analysis Based on Perturbations of a Aeriodic Stationary State, ASME 1992, *Japan-USA Symposium on Flexible Automation,* San Francisco, CA, July 1992, 2:1737-42.

Caumond A., Lacomme P., Moukrim A. and Tchernev N. (2009). An MILP for Scheduling Problems in an FMS with One Vehicle, *European Journal of Operational Research,* 199:706-722.

Chan F.T.S. and Chan H.K. (2004). Analysis of Dynamic Control Strategies of an FMS Under Different Scenarios. *Robotics and Computer Integrated Manufacturing,* 20:423-437.

Chow W.M. (1988). A Dynamic Job-Assignment Policy. *International Journal of Production Research,* 26(6):1073-87.

Denzler D.R., Boe W.J. and Duplaga E. (1987). An Experimental Investigation of FMS Rules under Uncertainty. *Journal of Operations Management,* 7:139-151.

El-rayah T.E. (1979). The Efficiency of Balanced and Unbalanced Production Line. *International Journal of Production Research,* 17:61-75.

Farkas A., Koltai T. and Stecke K.E. (1999). Workload Balancing Using the Concept of Operation Types. Working Paper, No. 99-002, Faculty Research, The University of Michigan Business School, Ann Arbor, MI, pp. 1-23.

Goyal S.K., Mehta K., Kodali R. and Deshmukh S.G. (1995). Simulation for Analysis of Scheduling Rules for a Flexible Manufacturing System. *Integrated Manufacturing Systems,* 6:21-26.

Gupta D. and Buzacott J.A. (1989). A Framework for Understanding Flexibility of Manufacturing Systems. *Journal of Manufacturing Systems,* 8(2):89-97.

Hayrinen T., Johnson M., Johtela T., Smed J. and Nevalainen O. (1998). Scheduling Algorithms for Computer-Aided Line Balancing in Printed Circuit Board Assembly. TUCS Technical Report, No. 212, Turku Centre for Computer Science, Turku, pp. 1-34.

Kim C.W., Tanchoco J.M.A., Koo P.H. (1997). Deadlock Prevention in Manufacturing Systems with AGV System: Banker's Algorithm Approach. *Journal of Manufacturing Science and Engineering,* 119:849-854.

Klahorst T.H. (1981). Flexible Manufacturing Systems: Combining Elements to Lower Costs, Add Flexibility. *Industrial Engineering,* 32(11):112-17.

Kosturiak J. and Gregor M. (1998). FMS Simulation: Some Experience and Recommendations. *Simulation Practice and Theory* 6, pp. 423-442.

Kumar N. and Shankar K. (2001). Comparing the Effectiveness of Workload Balancing Objectives in FMS Loading. *International Journal of Production Research,* 39(5):843-871.

Lee S. (2007). Locating Idle Vehicles in Tandem-Loop Automated Guided Vehicle Systems to Minimize the Maximum Response Time. *IEMS* 6(2): 125-135.

Meredith J.R. (1989). Managerial Lessons in Factory Automation: Three Case Studies in Flexible Manufacturing Systems. *Monograph* No. 4, Operations Management Association, pp. 1-77.

Mönch L., Prause M. and Schmalfuss V. (2001). Simulation-based Solution of Load-Balancing Problems in the Photolithography Area of a Semiconductor Wafer Fabrication Facility. Proceedings of the 2001 Winter Simulation Conference, Arlington, VA, pp. 1170-1177.

Phadke S.M. (1989). Quality Engineering Using Robust Design. Prentice Hall, Englewood Cliffs, N.J.

Pramod M., Garg S. (2006). Analysis of Flexibility Requirements under Uncertain Environments. *Journal of Modeling in Management,* 1(3):196-214.

Raghavendra B.V., Murthy A.N.N. (2010). Some Solution Approaches to Reduce the Imbalance of Workload in Parallel Machines while Planning in Flexible Manufacturing System. *International Journal of Engineering Science and Technology,* 2(5):724-730.

Raghavendra B.V., Murthy A.N.N. (2011). Workload Balancing in Identical Parallel Machine Scheduling while Planning in Flexible Manufacturing System Using Genetic Algorithm. *ARPN Journal of Engineering and Applied Sciences,* 6(1):49-55.

Rajakumar S., Arunachalam V.P., Selladurai V. (2004). Workflow Balancing in Parallel Machine Scheduling. *International Journal of Advance Manufacturing Technology,* 23:366-374.

Rajakumar S., Arunachalam V.P., Selladurai V., (2007). Workflow Balancing in Parallel Machines through Genetic Algorithm. *International Journal of Advance Manufacturing Technology,* 33:1212-1221.

Ranky P. (1983). The Design and Operation of FMS: Flexible Manufacturing Systems. IFS Publications Ltd, Bedford, 1983.

Ross E.A., Mahmoodi F. and Mosier C.T., (1996). Tandem Configuration Automated Guided Vehicle Systems: A Comparative Study. *Decision Sciences,* 27:81-102.

Saad S.M., and Byrne M.D. (1998). Comprehensive Simulation Analysis of a Flexible Hybrid Assembly System. *Integrated Manufacturing Systems* 9(3):156-167.

Sabuncuoglu I. and Hommertzheim D.L. (1992). Dynamic Dispatching for Scheduling Machines and Automated Guided Vehicles in a Flexible Manufacturing System. *International Journal of Production Research,* 30(5):1059-1079.

Shafiq S.I., Faheem M. and Ali M. (2010). Effect of Scheduling and Manufacturing Flexibility on the Performance of FMS. *Global Journal of Flexible Systems Management,* 11(3):21-37.

Stockton D. and Bateman N. (1995). Measuring the Production Range Flexibility of a FMS. *Integrated Manufacturing Systems,* 6(2):27-34.

Tunali S. (1996). Evaluation of Alternate Routing Policies in Scheduling a Job-shop Type FMS. *Computers and Industrial Engineering,* 32(2):243-240.

Yildirim M.B., Cakar T., Dogue U., Meza J.C. (2006). Machine Number, Priority Rule, and Due Date Determination in Flexible Manufacturing Systems Using Artificial Neural Networks. *Computers and Industrial Engineering,* 50:185-194.

Key Questions

1. How buffer capacities affect the performance of FMS?
2. Can the improvement in bottleneck workstation always improve the performance?
3. What are the methods to find the best factor level combinations for performance measures?

Ravindra Kumar is presently associated with Guru Premsukh Memorial College of Engineering, Delhi as an Assistant Professor in Mechanical and Automation Engineering department. Presently he is pursuing Ph. D. from Jamia Millia Islamia, Delhi. His areas of interest include flexible manufacturing systems, computer aided design and computer aided manufacturing. He is the corresponding author.

E-mail: ravi3000@gmail.com

Abid Haleem a Professor and Head of Mechanical Engineering and Coordinator of MBA (Evening) programme at Faculty of Engineering and Technology, Jamia Millia Islamia (A Central University by an Act of Parliament), New Delhi, India. Obtained Ph D from I I T Delhi in the area of 'Policy Planning'. Has more than eighty research papers to his credit, published in international and national journals. Has edited a book titled "Innovation, Flexibility and Technology Transfer", published by Tata McGraw Hill, India. His research interest are E-governance, Technology Management, Supply Chain Management, Flexible Systems and Systems Modeling etc. He is Regional Editor – Asia Pacific of Global Journal of Flexible Systems Management.

Suresh K. Garg is a Professor in Mechanical Engineering Department at Delhi Technological University, Delhi, India. His areas of interest include competitive strategies, JIT manufacturing systems, quality management, technology management and supply chain management. He has published sixty papers in international and national journals/conferences such as International Journal of Manufacturing Technology and Management, International Journal of Production Economics, Competitiveness Review, International Journals of Productivity and Quality Management, International Journal of Services and Operations Management, Journal of Modelling in Management, IIMB Management Review, Global Journal of Flexible Systems and Management and Productivity.

E-mail: skgarg63@yahoo.co.in

Dr. Rajesh K Singh is an Associate Professor at Indian Institute of Foreign Trade (IIFT), Delhi, India. He has published about 60 research papers in reputed international journals and conferences. His areas of interest include Competitiveness, Small Business Management, Quality Management and Supply Chain Management. He has published papers in journals such as Industrial Management and Data Systems, Singapore Management Review, International Journals of Productivity and Performance Management, International Journal of Automotive Industry and Management. Competitiveness Review: An International Journal, International Journals of Services and Operations Management, Global Journal of Flexible Systems and Management, International Journals of Productivity and Quality Management, South Asian Journal of Management, Productivity, IIMB Management Review and Productivity Promotion.

Surface To Surface Map Algorithm For Protein - Small Molecule Matching

Neha Gupta & Megha Bajaj

Information Technology, Delhi College of Engineering, Delhi, India
Institute of Molecular Bioscience, The University of Queensland, Brisbane, Australia
Email: neha.dce04@gmail.com, micro.megha@gmail.com

Abstract **-** Current methods for protein analysis are based on either sequence similarity or comparison of overall tertiary structure. These conserved primary sequences or 3-dimensional structures may imply similar functional characteristics. However, substrate or ligand binding sites usually reside on or near protein surface, so, similarly shaped surface regions could imply similar functions. Our current work includes development of an algorithm that would allow surface matching over specific regions on related proteins with an output equal to the match percentage between two proteins. Initial results indicate that we can successfully match a family of related active sites, and find their similarly shaped surface regions. This method of surface analysis could be extended to help us understand functional surface relationship between the proteins within which there is no relationship in sequence or overall structure.

Keywords- *Connolly Surface; K-mean clustering; Surface features;, Surface properties(shape index and radius of curvature)*

I. INTRODUCTION

Comparison of protein sequences and overall tertiary structures has added enormously to our understanding of structural, functional and evolutionary relationships between proteins. However, ligand binding sites usually occur on or near protein surface, so, similarly shaped surface regions could imply similar functions. Hence, comparing protein surfaces has power to reveal further functional relationships between proteins which might not be apparent from comparison of overall 3D structure. Various methods[1][2][3][4] have been developed describing shape properties of protein surfaces but they are not flexible enough to be able to recognize small variations caused to the protein surface due to conformational changes associated with mechanisms such as induced-fit. So, there is a need of an algorithm which estimates proteins surface similarity accurately, further contributing to our understanding of structural and functional relationships between proteins and, hence, become a powerful tool for prediction of function from structure.

The aim of the author was to develop an algorithm that would allow surface matching over specific regions on related proteins with an output equal to the match percentage between two proteins. For this, the author has implemented an algorithm which goes through various complex steps involving large number of mathematical calculations. In this paper, the steps involved and the results are listed.

II. STEPS INVOLVED

The algorithm used is four-phased executed sequentially i.e. output of one step is the input for the proceeding step. The four steps are:

1) To calculate the Connolly surface[5] of the 3D protein or the ligand binding site.

2) To compute the surface properties which include shape index and radius of curvature for each vertex on the Conolly Surface.

3) Select surface features on the basis of parent residues(the residues part of the surface to be compared)

4) To construct graphs for two proteins surfaces and compare them with each other. Aligning is done at the same time and the match percentage is calculated.

III. DEFINITIONS

A few definitions important for understanding the content of paper have been listed below:

A. Connolly Surface :

The solvent accessible surface(SAS) is the surface of protein which is in direct contact with the solvent. It is calculated by rolling a solvent ball over the protein and tracing the path which the center of the ball travels to form the SAS. In general, solvent accessible surface has many sharp crevices and sharp corners. In hope of obtaining a smoother surface, one can take the surface swept out by the front instead of the center of the solvent ball. This surface is the molecular surface (MS model), which is often called the Connolly's surface after Michael Connolly who developed the 1st algorithm for computing molecular surface [6].

B. Principal Curvatures(K_{max} and K_{min}):

In differential geometry, the two principal curvatures at a given point of a surface are the eigenvalues of the shape operator at the point. They measure how the surface bends by different amounts in different directions at that point.

C. Radius of Curvature :

A positive number, c , to specify the amount, or 'intensity' of the surface curvature. It is defined as the curvedness as the distance from the origin in the **(**K1,K2)- plane. 'The scaling is such that the curvedness equals the absolute value of the reciprocal radius in the case of sphere. The curvedness-is inversely proportional with the size of the object. Whereas the shape index scale is quite independent of the choice of a unit of length, the curvedness scale is not. Curvedness has the dimension of reciprocal length.'[16] It is given by this formula :

$$C = \frac{\left(k_{max}^2 + k_{min}^2\right)^{1/2}}{2}$$

where k_{max} and k_{min} are principal curvatures.

D. Shape Index :

It is a number ranging from -1 to 1 and is scale invariant. The shape index captures the intuitive notion of 'local shape' particularly well. It is given by this formula :

$$S = -2 \arctan \frac{k_{max} + k_{min}}{k_{max} - k_{min}}$$

where k_{max} and k_{min} are principal curvatures

and faces formed by joining three edges.

IV. DETAILED EXPLANATION OF STEPS

STEP 1: Generating the Connolly Surface

To compute the Connolly surface, an input file including a list of the atom centres in 3D space and radius of each defining the complete 3D structure of a protein is needed. For example, a pdb file has a list of atom centres and their radii which define the corresponding protein. The algorithm began by generating a Connolly surface for ligand binding site or on entire protein using MSMS program[7] which triangulates the Connolly surface and gives an output listing all the vertices of the triangulated surface.

.

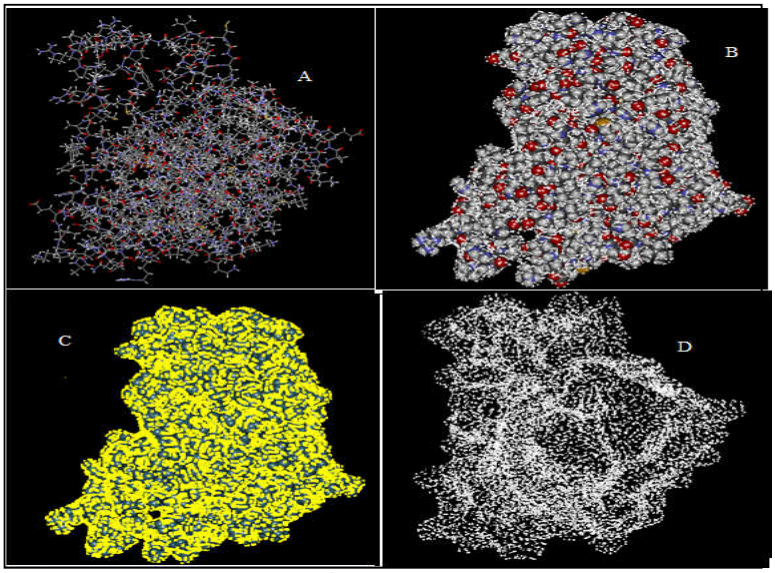

Figure 1 : a) Protein b,c) Connolly surface superimposed on protein d) Connolly Surface

. The radius of the probe can also be changed according to the precision required while running the executable of MSMS program. The calculation performed by the author was done by taking probe radius 1.4 Angstrom.

STEP 2: To compute the surface properties which include shape index and radius of curvature for each vertex on the Conolly Surface

The algorithm proceeds by calculating the surface shape properties(shape index and radius of curvature) at each of the vertices on the Connolly surface(calculated in the previous step) . This step is accomplished by using the GTS-GNU Triangulated Surface library[15] which calculates the principal curvatures at a surface patch , k_{min} and k_{max}[16]. Shape index (S) and Radius of curvature(R) in terms of principal curvatures is given by the following formula :

$$S = -2\arctan\frac{k_{max}+k_{min}}{k_{max}-k_{min}} \text{ and}$$

$$R = \frac{\left(k_{max}^2 + k_{min}^2\right)^{1/2}}{2}$$

‘‘The shape index varies from −1 to 1 and describes the local shape at a surface point independent of the scale of the surface. A convex surface point with equal principal curvatures has a shape index of 1. A concave surface point with equal principal curvatures has a shape index of −1. A saddle surface point with principal curvatures of equal magnitude and opposite signs has a shape index of 0’’ (Duncan and Olson, 1993b).

Sample data obtained in this step is listed in Table 1.

STEP 3 : Select surface features on the basis of parent residues(the residues part of the surface to be compared)

In order to match the two surfaces, k-mean clustering [10] was performed where each chosen surface feature corresponds to a cluster. To decide whether a triangulated vertex should be added to a cluster or not, constraints were applied on shape index (S) and radius of curvature (R) after adding the new vertex. The constraints applied were as follows:

1. S-variance of cluster size(x) is less than 0.0453*pow(x, 0.0528)
2. R-variance of cluster size (x) is less than 0.1 if x <200, else less than 0.15
3. All the points in a cluster should be connected as per edge-criterion.

Also, the author introduced the residues restriction: User can give list of residues which are important. Now when the surface points are going to KMean clustering program, only the points which belong to the marked residues would be considered. The number of clusters can be decided at the run time to make sure atleast one cluster is assigned to each of the important residues.

If the constraints were not met, newly added vertex was removed from the cluster. In this step, clusters equal to the number of chosen features were obtained each having a 3D location, corresponding to the 3D location of the centre (mean) of the cluster. Each cluster also has an S and R value associated with it.

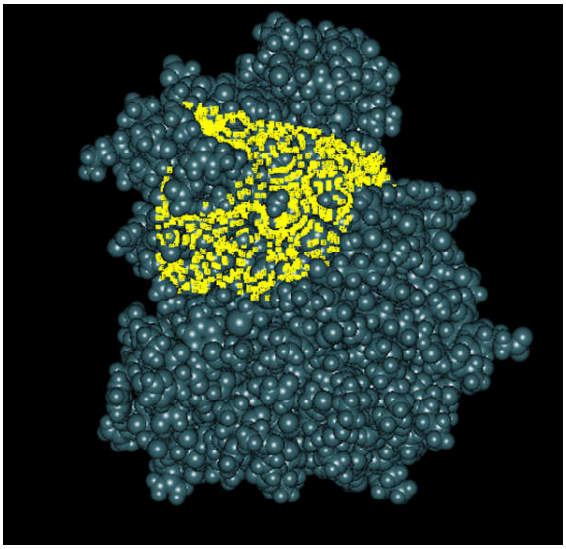

Figure 2 : Ligand binding Site for comparison

STEP 4 : To construct graphs for two proteins surfaces and compare them with each other. Aligning is done at the same time and the match percentage is calculated.

A mathematical graph with nodes as the cluster centres marked with properties S and R was constructed [14]. Edges comprised of an all-to-all joining of nodes with separation equal to the 3d distance in space. For both the proteins, 2 such graphs were formed and the maximal common sub-graph indicated a measure of the similarity between the two proteins. In this case, a match requires distances and shape properties to match within user-defined tolerances (typically 1.5 A_ for distances).

Greater tolerances allow matches between more distantly related surfaces and account for surface flexibility. Lesser tolerances will have more accuracy, but at the same time over-precision lead to anomalous results.

TABLE I : SAMPLE VERTEX COORDINATES AND SURFACE PROPERTIES

X-coordinate	Y-coordinate	Z-coordinate	Shape index	Radius of curvature
43.1600	57.2280	26.2730	-0.3100	0.2953
43.1630	57.2150	26.2790	-0.4363	0.2875
44.2170	57.1240	25.5320	-0.7292	0.3530
22.5130	48.6460	29.6830	-1.0000	0.2071
21.4070	48.2750	30.3250	-0.3745	0.0848

The product graph[8] was first calculated which was then used to find the maximal common subgraph using the Bron and Kerbosch algorithm [9] to detect cliques. When a match was discovered by the method above, the surfaces were superimposed in 3D to align the two surfaces. This was done using matrix algebra [11][12][13] to obtain the best rotation to relate the two sets of points.

RESULT: The proposed algorithm is a comprehensive approach to match selected parts or regions of two protein surfaces. This algorithm has been implemented and results found were in coherence with the expected results. Specific ligand binding sites or patches on protein surfaces can be successfully compared using the proposed algorithm.

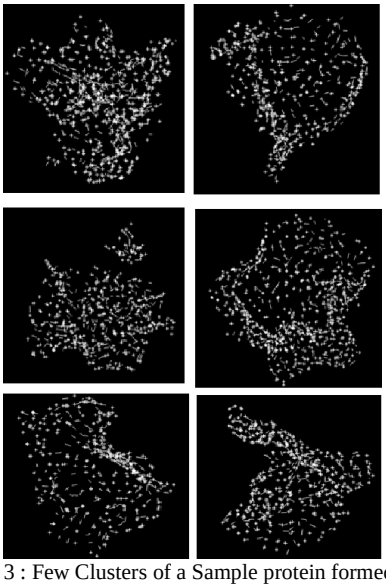

Figure 3 : Few Clusters of a Sample protein formed after applying K-mean clustering algorithm and applying constraints mentioned

The match percentage calculated can be used to identify functionally related surfaces in much more distantly related proteins.

FUTURE SCOPE: Further scope includes testing of proteins in which there is a functional surface relationship but no relationship in sequence or overall structure, and different types of functional sites. Also, chemical descriptors to the surface, including charge, hydrophobicity, and residue/atom identity can be added to the algorithm which will increase the power of our method in describing functional features of proteins.

REFERENCES

[1] Orengo, C.A., Taylor, W.R., 1996. Methods Enzymol. 266,617–635.J. Clerk Maxwell, A Treatise on Electricity and Magnetism, 3rd ed., vol. 2. Oxford: Clarendon, 1892, pp.68–73.

[2] Holm, L., Sander, C., 1993. J. Mol. Biol. 233, 123–138.

[3] Alexandrov, N.N., 1996. Protein Eng. 9, 727–732.

[4] Michel F. Sanner,Arthur J. Olson,Jean-Claude Spehner, Reduced Surface: An Efficient Way to Compute Molecular Surfaces

[5] Koch, I., Lenauer, T., Wanke, E., 1996. J. Comp. Biol. 3,289–306.Electronic Publication: Digital Object Identifiers (DOIs): Article in a journal:

[6] Bron, C., Kerbosch, J., 1971. Commun. ACM 16 (9), 1973.

[7] David M. Mount, KMlocal: A Testbed for *k*-means Clustering Algorithms

[8] Russell, R.B., Barton, G.J., 1992. Proteins 14, 309–323.

[9] McLachlan, A.D., 1972. Acta Crystallogr., Sect. A 28, 656.

[10] Kabsch, W., 1978. Acta Crystallogr., Sect. A 34, 827–828.

[11] Harary, F., 1967. Graph Theory. Addison–Wesley, London

[12] http://gts.sourceforge.net/

[13] Jan J Koenderink and Andrea J van Doorn, Surface shape and curvature scales

◈◈◈